

Multispectral Indices for Wildfire Management

Afonso Oliveira, Filipe Moutinho, Nuno Fachada, João P. Matos-Carvalho

Abstract—The increasing frequency and severity of wildfires requires advanced methods for effective surveillance and management. Traditional ground-based observation techniques often struggle to adapt to rapidly changing fire behavior and environmental conditions. This paper examines the application of multispectral aerial and satellite imagery in wildfire management, emphasizing the identification and analysis of key factors influencing wildfire behavior, such as combustible vegetation and water features. Through a comprehensive review of current literature and the presentation of two practical case studies, we assess various multispectral indices and evaluate their effectiveness in extracting critical environmental attributes essential for wildfire prevention and management. Our case studies highlight several indices as particularly effective for segmentation and extraction: NDVI for vegetation, MNDWI for water features, and MSR for artificial structures. These indices significantly enhance wildfire data processing, thereby supporting improved monitoring and response strategies.

Index Terms—Wildfires, multispectral imaging, multispectral indices, remote sensing,

I. INTRODUCTION

The effective monitoring and maintenance of forests and other vegetated regions are crucial for mitigating the rising risks associated with extreme natural events [1]. The growing frequency of extreme heatwaves, lightning storms, and droughts has revealed their destructive potential, especially in terms of escalating the incidence of severe wildfires [2], [3]. To address these emerging challenges, it is necessary to develop and adopt innovative strategies that improve the preparedness and response capabilities of civil authorities [4].

Current methods for wildfire surveillance, analysis, and management often fail to address the increasing severity of wildfires. Traditional approaches, such as ground-based observations and manual data collection, cannot keep pace with rapidly changing fire behavior and environmental conditions [5], [6]. These methods are typically slow to deploy, hindering timely responses to emerging threats. Additionally,

Afonso Oliveira is with Lusófona University and COPELABS, Campo Grande 376, 1749-024 Lisbon

Filipe Moutinho is with NOVA School of Science and Technology, NOVA University Lisbon, Largo da Torre, Caparica, 2829-516, Setúbal, Portugal; and Center of Technology and Systems (UNINOVA-CTS) and Associated Lab of Intelligent Systems (LASI), 2829-516 Caparica, Portugal

Nuno Fachada is with COPELABS, Campo Grande 376, 1749-024 Lisbon; and Center of Technology and Systems (UNINOVA-CTS) and Associated Lab of Intelligent Systems (LASI), 2829-516 Caparica, Portugal

João P. Matos-Carvalho is with LASIGE, Faculdade de Ciências, Universidade de Lisboa, 1749-016 Lisboa, Portugal; COPELABS, Campo Grande 376, 1749-024 Lisbon; and Center of Technology and Systems (UNINOVA-CTS) and Associated Lab of Intelligent Systems (LASI), 2829-516 Caparica, Portugal

This work was financed by the Portuguese Agency FCT (Fundação para a Ciência e Tecnologia), in the framework of projects UIDB/00066/2020, UIDB/04111/2020 and CEECINST/00147/2018/CP1498/CT0015

many regions rely on outdated predictive models that lack integration with recent climate data and evolving vegetation patterns, resulting in inaccurate risk assessments [7].

Remote sensing technologies and satellite imagery have significantly improved wildfire monitoring through higher spatial and temporal resolutions. However, challenges in data processing, integration, and analysis persist, limiting the speed and effectiveness of decision-making [8]. This paper examines the application of multispectral aerial and satellite imagery in wildfire management. Specifically, it examines the most effective multispectral indices for extracting and segmenting key factors that influence wildfire behavior, including combustible vegetation, water features, and infrastructure. These factors form the foundation for effective prevention and management strategies. In addition, the paper highlights the versatility and utility of these indices in addressing common challenges within the field, while providing actionable insights for optimizing the analysis of vegetated areas. Ultimately, this work aims to serve as a timely and comprehensive resource for researchers and professionals engaged in wildfire prevention and management, such as fire ecologists, remote sensing specialists, forest managers, environmental scientists and emergency planners.

This paper is organized as follows. Section II introduces the concept of multispectral imaging, offering an overview of the indices reviewed in this study and discussing their relevance and potential. In Section III, we highlight key metrics for evaluating multispectral indices. Section IV focuses on various aspects of feature extraction using multispectral indices, including the extraction of vegetation (Subsection IV-A) and soil (Subsection IV-B) attributes, the mapping of water features (Subsection IV-C) and artificial structures (Subsection IV-D), and the estimation of burnt areas post-fire (Subsection IV-E). In Section V, we present two practical case studies illustrating the application of the discussed multispectral. Building on the information and literature reviewed, Section VI provides several recommendations for the use of multispectral indices and techniques across different scenarios. The paper concludes with Section VII, which summarizes the key points addressed throughout this study.

II. MULTISPECTRAL IMAGING

Multispectral imaging is a technique that captures image data across multiple wavelengths in the electromagnetic spectrum. By dividing the spectrum into discrete bands, it enables the detection and analysis of specific spectral signatures emitted or reflected by various land cover types. Although the precise spectral range of each band varies by instrument, band names and spectral intervals typically follow standardized conventions.

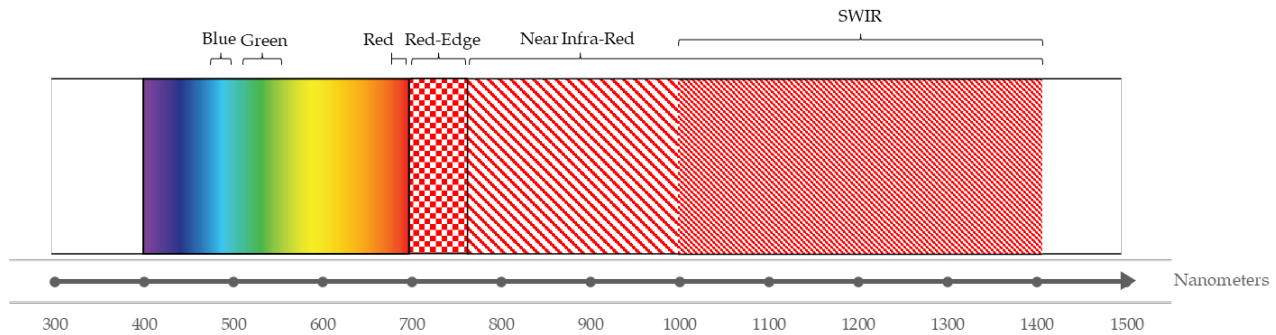


Fig. 1. Electromagnetic spectrum with approximate location of relevant bands.

Multispectral imaging captures a limited number of spectral bands, usually ranging from 3 to 10, making data acquisition and processing fast and cost-effective. This simplicity and efficiency make it well-suited for broad applications such as agriculture, forestry, and land cover mapping, where general spectral differences are sufficient. However, its relatively low spectral resolution may overlook subtle spectral features, limiting its ability to distinguish between materials with similar spectral properties. In contrast, hyperspectral imaging captures hundreds of narrow, contiguous spectral bands [9], providing much higher resolution that allows for precise identification and differentiation of similar materials. This capability is ideal for more complex applications, such as mineral exploration, environmental monitoring, and medical diagnostics, where detailed spectral information is crucial. However, the increased data volume in hyperspectral imaging leads to slower data acquisition and processing, and higher storage costs. Additionally, managing and analyzing hyperspectral data requires significant computational and technical resources, further increasing its complexity and expense. Overall, multispectral imaging is more suitable for wildfire management than hyperspectral imaging because it provides essential data across a few broad spectral bands. This makes it faster, less data-intensive, and more practical for real-time monitoring of large areas.

Within multispectral imaging, the blue, green, red, red-edge, and near-infrared (NIR) spectral bands stand out in terms of cost and availability, making them suitable not only for wildfire management [10], but also for a wide range of applications, such as fire ecology [11], precision agriculture [12], and land cover assessment [13]. Figure 1 provides a visual illustration of these and other relevant bands, such as those in the Short-Wave Infrared (SWIR) spectrum, along with their approximate ranges.

Depending on the goal, these bands can be utilized in various ways. For example, the red-edge (700 to 750 nm) [14] and NIR (750 to 1400 nm) [15], [16] bands can provide valuable insights into the structural and physiological characteristics of vegetation. These are particularly useful for detecting subtle changes in plant health and identifying stress factors.

While single-band analysis may be sufficient for simpler cases, many applications require more advanced approaches, such as generating and analyzing Color-Infrared (CIR) imagery or computing multispectral indices. CIR imagery con-

verts NIR data into the visible spectrum by combining green, red, and NIR bands. This technique provides a valuable resource that can be analyzed independently or subjected to further processing [17], [18]. CIR imagery enables more precise assessments of vegetation distribution, density, and health, while also distinguishing between vegetation, soils, water bodies, and certain man-made structures [19].

In CIR imagery, healthy, dense vegetation appears in bright red, gradually transitioning to shades of pink as vegetation health declines. Dead vegetation is represented by hues of green, cyan, and tan. Bare soil colors vary depending on composition: clay soils appear as darker shades of tan and cyan, while sandy soils are lighter in tone, ranging from tan to gray or even white. The natural appearance of soil in CIR imagery can be influenced by factors such as moisture content and organic material concentration [19]. Water bodies are depicted in various shades of blue and black, reflecting their clarity, except in the case of shallow streams, where the appearance directly corresponds to the soil composition of the stream bed. The appearance of man-made structures varies based on their material composition. For instance, gravel roads tend to be lighter, while asphalt roads appear dark blue or black [19].

Multispectral indices offer a more refined approach to extract insights from multispectral data. These indices enhance specific image bands to create composite images that highlight particular features, thereby improving both the quantity and quality of the data. Various classes of indices have been developed for diverse applications, ranging from vegetation-focused indices to specialized indices for soil content assessment [20] and oil slick detection [21]. Nonetheless, despite rapid advancements in this field, some indices have maintained their foundational importance and continue to be highly relevant.

Table I provides an overview of the indices discussed in this work, categorized by their general formulaic configuration and function, along with the respective formulas and references to the studies that introduced them. These indices will be explored in greater detail throughout the paper. Additionally, Table XI (in Appendix A) presents an alphabetically organized list of acronyms and full names for all indices discussed.

TABLE 1

MULTISPECTRAL INDICES GROUPED BY FORMULAIC CONFIGURATION AND FUNCTION, THEIR RESPECTIVE FORMULA, AND A REFERENCE TO THE STUDY THAT INTRODUCED THEM. I - SIMPLE GREENNESS INDICATORS; II - ANTHOCYANIN REFLECTANCE INDICES; III - ENHANCED VEGETATION INDICES; IV - SOIL-ADJUSTED VEGETATION INDICES; V - MODIFIED BARE SOIL INDICES; VI - TERRAIN ADJUSTED VEGETATION INDEX; VII - NDHD COMPOSITES; VIII - VEGETATION INDEX BASED ON UNIVERSAL PATTERN DECOMPOSITION METHOD (VIUPD); IX - WATER/MOISTURE EXTRACTION INDICES; X - BURNT AREA EXTRACTION INDICES; XI - ARTIFICIAL SURFACE INDEX AND COMPONENTS; XII - ROAD EXTRACTION INDICES;

Group	Index	Formula	Ref.	Group	Index	Formula	Ref.	
I	SR	$\frac{\rho_{NIR}}{\rho_R}$	[22]	VI	TAVI	$\frac{\rho_{NIR} + f(\Delta) \times (M_R - \rho_R)}{\rho_B}$	[23]	
	NDVI	$\frac{\rho_{NIR} - \rho_R}{\rho_{NIR} + \rho_R}$	[24]	VII	NDHD	$\frac{\rho_{HS} - \rho_{DS}}{\rho_{HS} + \rho_{DS}}$	[25]	
	DVI	$\rho_{NIR} - \rho_R$	[26]		NHVI2	$\rho_{NIR} \times \rho_{NDHD}$	[27]	
	RDVI	$\frac{\rho_{NIR} - \rho_R}{\sqrt{\rho_{NIR} + \rho_R}}$	[28]		HSV1	$\rho_{NIR} \times \rho_{NDHD}$	[27]	
	MSR	$\frac{\rho_R}{\sqrt{\frac{\rho_{NIR} + 1}{\rho_R}}}$	[29]		HEVI2	$\rho_{NIR} \times \rho_{NDHD}$	[27]	
	GNDVI		$\frac{\rho_{NIR} - \rho_G}{\rho_{NIR} + \rho_G}$	[30]	VIII	VIUPD	$C_V - 0.12 \times C_S - C_4$	[31]
		GARI	$\frac{\rho_{NIR} + \rho_G - \gamma(\rho_B - \rho_R)}{\rho_{NIR} + \rho_G - \gamma(\rho_B - \rho_R)}$	[30]	IX	NDWI	$\frac{C_W + C_V + C_S}{\rho_G - \rho_{NIR}}$	[32]
		NDRE	$\frac{\rho_{NIR} - \rho_{PRE}}{\rho_{NIR} + \rho_{PRE}}$	[33]		NDMI	$\frac{\rho_{NIR} - \rho_{SWIR}}{\rho_{NIR} + \rho_{SWIR}}$	[32]
		GDVI	$\rho_{NIR} - \rho_G$	[34]		MNDWI	$\frac{\rho_G + \rho_{SWIR}}{\rho_G - \rho_{SWIR}}$	[35]
		GRVI	$\frac{\rho_G}{1 - (\rho_{NIR} - \rho_R)}$	[36]	X	NBR	$\frac{\rho_{NIR} - \rho_{SWIR}}{\rho_{NIR} + \rho_{SWIR}}$	[37]
IDVI		$\frac{1 - (\rho_{NIR} - \rho_R)}{1 - (\rho_{NIR} - \rho_R)}$	[38]		BAI	$(0.12 - R)^2 + (0.06 - NIR)^2$	[39]	
II		ARI	$\frac{1}{\rho_G - \rho_{RE}}$	[40]		NBRT1	$\frac{\rho_{NIR} - \rho_{SWIR} \left(\frac{\rho_{Thermal}}{10000} \right)}{\rho_{NIR} + \rho_{SWIR} \left(\frac{\rho_{Thermal}}{10000} \right)}$	[41]
		MARI	$\rho_R \times \rho_R$	[40]	XI	ASI	$\phi(\text{AF}) \times \phi(\text{VSF}) \times \phi(\text{SSF}) \times \phi(\text{MF})$	[42]
		EVI	$\frac{2.5 \times (\rho_{NIR} - \rho_R)}{\rho_{NIR} + 6 \times \rho_R - 7.5 \times \rho_B + 1}$	[43]		ASI (Alt.)	$\frac{1}{16} \times (\text{AF} + 1) \times \text{VSF} \times \text{SSF} \times (\text{MF} + 1)$	[42]
III		EVI2	$\frac{\rho_{NIR} + 2.4 \times \rho_B + 1}{\rho_{NIR} + 2.4 \times \rho_B + 1}$	[44]		AF	$\frac{\rho_{NIR} - \rho_B}{\rho_{NIR} + \rho_B}$	[42]
	SAVI	$1.5 \times \frac{\rho_{NIR} - \rho_R}{\rho_{NIR} + \rho_R + 0.5}$	[45]		VSF	$1 - (\text{NDVI} \times \text{MSAVI})$	[42]	
	MSAVI	$\frac{2 \times \rho_{NIR} + 1 - \sqrt{(2 \times \rho_{NIR} + 1)^2 - 8 \times (\rho_{NIR} - \rho_{RED})}}{2}$	[46]		SSF	$1 - \text{EMBI}$	[42]	
IV	OSAVI	$1.126 \times \frac{\rho_{NIR} - \rho_R}{\rho_{NIR} + \rho_R + 0.126}$	[47]		MF	$\frac{(\rho_B + \rho_G) - (\rho_{NIR} + \rho_{SWIR})}{(\rho_B + \rho_G) + (\rho_{NIR} + \rho_{SWIR})}$	[42]	
	MBI	$\frac{\rho_{SWIR1} - \rho_{SWIR2}}{\rho_{SWIR2} - \rho_{NIR}} + 0.5$	[48]	XII	REI	$\frac{\rho_{NIR} - \rho_B}{\rho_{NIR} + \rho_B \times \rho_{NIR}}$	[49]	
	EMBI	$\frac{\text{MBI} - \text{MNDWI} - 0.5}{\text{MBI} + \text{MNDWI} + 1.5}$	[42]		RI	$1 - \frac{\rho_{NIR} + \rho_B \times \rho_{NIR}}{\rho_{SWIR} + \rho_{NIR} + \rho_B}$	[50]	

$\rho_B, \rho_G, \rho_R, \rho_{RE}, \rho_{NIR}, \rho_{SWIR}$: Reflectance for the Blue, Green, Red, Red-Edge, NIR, and SWIR band reflectances, respectively.

$\rho_{Thermal}, \rho_{HS}, \rho_{DS}$: Thermal, Hotspot, and Darkspot reflectances, respectively.

C_V, C_S, C_W, C_Y : Vegetation, Soil, Water, and Yellow reflectance coefficients, respectively.

$f(\Delta)$: Topography adjusting coefficient.

M_{RED} : Maximized Red band reflectance

$\phi(\#)$: Min-Max normalization function based on the entire image.

III. INDEX COMPARABILITY AND METRICS

To effectively compare solutions, it is essential to evaluate their performance relative to one another. Studies may employ various methods to assess performance, often influenced by the chosen methodology or the author’s preferences. One commonly used metric is *accuracy*, which measures how closely a result aligns with the true or expected value. Higher accuracy indicates more correct and reliable predictions, measurements, or outcomes. Accuracy is typically expressed as a percentage, with 100% indicating that the method perfectly describes or predicts the outcomes without any errors or discrepancies. Another important metric is *sensitivity*, which evaluates how variations in a particular variable or condition influence the outcome. Sensitivity is crucial for assessing a method’s robustness and reliability under varying circumstances. In statistical contexts, accuracy and sensitivity are commonly defined using the following formulas:

$$\text{Accuracy} = \frac{TP + TN}{TP + TN + FP + FN}$$

$$\text{Sensitivity} = \frac{TP}{TP + FN}$$

where *TP* denotes true positives, *TN* refers to true negatives, *FP* represents false positives, and *FN* corresponds to false negatives. For example, in the context of pixel-wise image analysis, these metrics could evaluate the classification of individual pixels. A *TP* occurs when a pixel that genuinely belongs to the target class is correctly identified. A *TN* is when a pixel that does not belong to the target class is accurately classified as non-target. A *FP* arises when a pixel that does not belong to the target class is incorrectly classified as part of it, leading to over-detection or false alarms. Conversely, a *FN* occurs when a pixel that belongs to the target class is misclassified as non-target, resulting in an omission or missed detection.

However, beyond accuracy and sensitivity, other metrics are often used for comparing indices. These metrics, along with concise descriptions of their interpretations and expected value ranges, are summarized in Table II.

The R^2 value is a metric that reflects how well a model explains the variance in the dependent variable, with its range spanning from 0 to 1. A higher R^2 indicates that the model provides a closer fit to the observed data. In contrast, the Root Mean Square Error (RMSE) measures the average prediction error of a model. RMSE values range from 0 to $+\infty$, and lower values indicate that the model’s predictions are more aligned with the observed data.

The Mean Intersection over Union (MIoU) is another important metric, particularly used in boundary and segmentation tasks. It evaluates the overlap between predicted regions and the ground truth, with values ranging from 0 to 1, where higher values indicate more precise segmentation performance.

Statistical tests provide a rigorous framework for evaluating differences in data, ensuring that observed variations are not merely the result of random fluctuations. In the context of multispectral indices and remote sensing, the choice of statistical test depends on the characteristics of the data and the specific

TABLE II
COMMON METRICS FOR COMPARING MULTISPECTRAL INDEXES, THEIR EXPECTED RANGES, AND INTERPRETATION.

Acronym	Name	Range	Interpretation
—	Accuracy	$[0, 1]^a$	▲
—	Sensitivity	$[0, 1]^a$	▲
R^2	Coefficient of Determination	$[0, 1]$	▲
RMSE	Root-Mean-Square Deviation	$[0, +\infty]^a$	▼
MIoU	Mean Intersection of Union	$[0, 1]$	▲
t-test	Student’s t-Test	$[0, 1]^b$	▼
ANOVA	Analysis of Variance	$[0, 1]^b$	▼
MWU	Mann-Whitney U Test	$[0, 1]^b$	▼
KW	Kruskal-Wallis Test	$[0, 1]^b$	▼
McNemar	McNemar Test	$[0, 1]^b$	▼
JMD	Jeffries–Matusita Distance	$[0, \sqrt{2}]^a$	▲
TD	Transformed Divergence	$[0, 2]^a$	▲
SDI	Spectral Discrimination Index	$[-\infty, \infty]^a$	▲

▲ A higher value is typically better.

▼ A lower value is typically better.

^a Sometimes expressed as a percentage.

^b Each statistical test returns a specific value (*t*-statistic, *F*-statistic, *U*-statistic, *H*-statistic, and χ^2 , respectively), along with a *p*-value for interpretation. *p*-values < 0.01 and < 0.05 are commonly used thresholds for statistical significance.

research objectives, with each test yielding a distinct metric or value. These test usually also generate a *p*-value. A *p*-value expresses the probability of obtaining results as extreme as the observed data, assuming the null hypothesis is true. A small *p*-value (often set at a threshold of 0.05 or 0.01) suggests that the observed result is statistically significant, implying it is unlikely to have occurred under the null hypothesis. In the context of multispectral indices, *p*-values help assess the statistical significance of differences in spectral data across different land cover types, vegetation health, or soil moisture levels. For instance, *p*-values can be used to determine whether observed changes in specific spectral bands (such as SWIR or NIR) between two time periods are statistically significant, supporting conclusions about vegetation stress, fire severity, or water content with more confidence.

In the context of multispectral image analysis, the Student’s *t*-Test is commonly used to compare the mean values of a spectral index between two independent or paired conditions, assuming normality. It returns a *t*-statistic, which measures the difference between group means relative to variability, and a *p*-value. When comparing more than two groups, Analysis of Variance (ANOVA) determines whether significant differences exist among them. It returns an *F*-statistic, reflecting the ratio of variance between groups to variance within groups. For non-normally distributed data, the Mann-Whitney U Test serves as a non-parametric alternative to the *t*-test, while the Kruskal-Wallis Test extends this approach to multiple groups. These tests return a *U*-statistic or *H*-statistic, respectively, along with a *p*-value, indicating whether distributions significantly differ. Finally, the McNemar Test is applied to paired categorical data, making it useful in classification accuracy assessments and land cover change detection. It returns a χ^2 statistic (or an exact *p*-value in small samples), assessing whether the proportion of changes between categories is statistically significant.

Separability metrics, including the Jeffries–Matusita Distance (JMD) [51], [52], Transformed Divergence (TD) [53], and Spectral Discrimination Index (SDI) [54], are commonly used to evaluate classification performance. Separability refers to how well different classes within a dataset can be distinguished from one another. The JMD quantifies the statistical distance between two probability distributions by emphasizing their overlapping areas. The TD measures the divergence between distributions but applies a transformation to ensure that the values are bounded. The SDI, on the other hand, assesses class separability based on spectral response patterns, highlighting differences in spectral reflectance. While the JMD and TD primarily focus on probabilistic separability, the SDI is more tailored to the spectral characteristics, making it especially relevant in remote sensing applications. In all three measures, higher values generally suggest greater separability between classes, indicating better performance in discriminating between different categories.

IV. FEATURE EXTRACTION

Multispectral indices are essential tools in remote sensing for feature extraction, as they enable the identification and analysis of specific surface characteristics. These characteristics serve as key data inputs for wildfire prediction algorithms, providing critical information for accurate forecasting. Four common characteristics have been identified as useful for such algorithms [55], [56], [57]: the distribution and composition of vegetation (Subsection IV-A) and soil (Subsection IV-B), which typically constitute the primary sources of fuel; the arrangement of water features (Subsection IV-C), which can serve as natural fire barriers; the placement of man-made structures (Subsection IV-D), which can affect the fire’s spread and must thus be considered when formulating wildfire management plans. Post-fire measures are also highly relevant. In particular, the assessment of burnt areas is instrumental in damage analysis, rehabilitation, and reforestation efforts. Consequently, this factor is examined in Subsection IV-E.

Figure 2 depicts an example process flow for extracting wildfire-related insights using multispectral indices. These insights help understand fire growth and movement patterns, which in turn can inform strategies for land management, including optimal locations for firebreaks, prescribed burns, fuel reduction programs, and evacuation plans.

A. Vegetation

Vegetation plays an essential role as a fuel source in wildfire behavior. Its composition, quantity, spatial arrangement, and moisture content directly impacts the intensity, spread, and duration of wildfires. Vegetation indexes are assessed based on their performance in distinguishing different vegetation densities (density performance), resistance to terrain reflection artifacts (topographic resistance), and resistance to atmospheric effects (atmospheric resistance).

The effectiveness of a vegetation index in assessing vegetation coverage relies on its ability to accurately measure density. The most commonly utilized vegetation indexes are those that measure greenness, leveraging the reflectance and

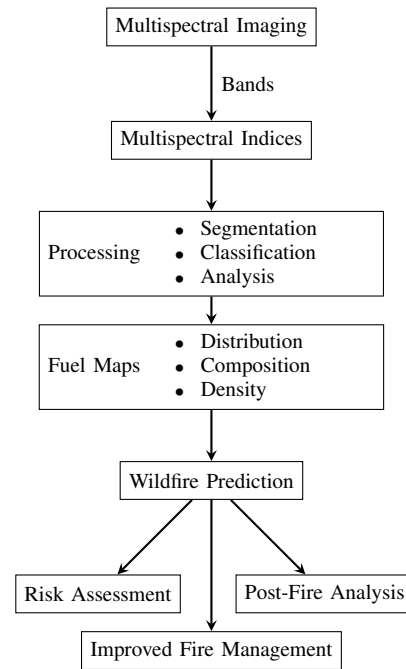


Fig. 2. Feature extraction for wildfire prediction using multispectral indices.

absorption properties of chlorophyll pigments to highlight vegetation details, as seen with NDVI [24]. However, there are also indices that focus on alternative pigments, such as the ARI [40] and the MARI [40] indices, which target anthocyanin pigments that typically impart blue, red, or purple hues to vegetation. The effectiveness of an index is closely linked to the density of pigment-rich vegetation in a specific area, making it less effective in regions where vegetation lacks these pigments.

Topographic and atmospheric factors can have a strong impact on the accuracy and reliability of vegetation indices. Topographic considerations include the influence of terrain features, such as slopes and shadows, which can affect sunlight availability and alter reflectance values. Atmospheric factors, on the other hand, are caused by components like aerosols, water vapor, and clouds, which scatter and attenuate solar radiation, leading to errors in reflectance measurements. Techniques such as topographic [58], [59] and atmospheric correction [60], [61], [62] algorithms can mitigate these issues, thereby enhancing the accuracy of vegetation indices. Table III provides a summary of the most effective indices for extracting vegetation attributes, highlighting their specific strengths.

When working with multispectral indices, even widely used ones, it is necessary to take into account their limitations. In terms of density performance, NDVI has been found to saturate in highly vegetated areas and produce inconsistent results in very arid regions [63]—with NDRE [33] being a possible alternative for the latter case [64]. Similarly, SAVI [45] faces challenges in accurately estimating vegetation in areas with a heterogeneous canopy [27].

Both the IDVI [38] and the VIUPD [31] indexes have demonstrated their ability to overcome some of NDVI’s limitations. IDVI shows insensitivity to leaf biochemical pa-

TABLE III
MULTISPECTRAL INDICES FOR VEGETATION ATTRIBUTE EXTRACTION.

Index	Density			Resistance		HI
	Low	Med.	High	Top.	Atm.	
NDVI	✓	✓		✓		✓
SAVI	✓	✓		✓		
RDVI		✓	✓		✓	
EVI		✓	✓	✓	✓	
NDWI	✓	✓	✓			✓
NDRE	✓	✓		✓		
EVI2		✓	✓	✓	✓	
VIUPD	✓	✓	✓			✓
TAVI	✓	✓		✓		
IDVI		✓	✓	✓		
NHVI2	✓	✓	✓			
HSVI	✓	✓	✓			
HEVI2	✓	✓	✓			

Top.: Topographic; Atm.: Atmospheric.

HI: Can be used as an health indicator.

rameters and a wider variation range compared to NDVI, resulting in more stable results. Similarly, the VIUPD method demonstrates a broader domain range and higher sensitivity to vegetation density, leading to superior performance in areas with high vegetation cover. Additionally, VIUPD also displays higher sensitivity to vegetation health and CO₂ concentration.

The methodology employed by VIUPD is uncommon, as it builds upon the Universal Pattern Decomposition Method (UPDM) [65]. VIUPD was developed as a redefinition of a revised vegetation index, also rooted in UPDM [66]. Despite the apparent complexity involved in calculating its coefficients, these can be computed using a structured three-step process [67], which greatly simplifies the calculations.

To improve the accuracy and applicability of SAVI in estimating vegetation in a heterogeneous canopy, the NDHD [25] composites—NHVI2 [27], HSVI [27], and HEVI2 [27]—were developed. These indices are calculated through the multiplication of a base index—NDVI, SAVI and EVI2 [27]—by the aforementioned NDHD. The latter represents the distribution of foliage in a canopy and its derived indices generally performed well when compared to SAVI and other commonly used multispectral vegetation indices, demonstrating higher performance in heterogeneous canopy regions and resistance to soil-noise effects [27].

Zhou et al. [68] consider topographic resistance as a notable characteristic shared by ratio indices, such as NDVI, NDWI [32], and NDRE. These indices—derived from low complexity ratios—have been observed to partially mitigate the influence of topographic variations, especially when compared to non-ratio indices like EVI [43], [68]. The issue of atmospheric resistance can also be minimized by various indices, such as RDVI [28], which offers additional mitigation against specific solar geometry distortions [69]. In addition to RDVI, the EVI and EVI2 indices are also robust in the presence of atmospheric interference.

The TAVI [23] index was developed taking topographic resistance into account. It addresses the high correlation between the solar incidence cosine and conventional vegetation indices that can lead to a loss of accuracy [23]. TAVI introduces two

TABLE IV
SOME LAI ESTIMATION APPROACHES. ADAPTED FROM [74].

Base	Formula	Ref.
NDVI	$9.519 \times \text{NDVI}^3 - 0.1204 \times \text{NDVI}^2 + 1.236 \times \text{NDVI} - 0.257$	[78]
	$4.9 \times \text{NDVI} - 0.46$	[79]
	$0.0287 \times e^{0.081 \times \text{NDVI}}$	[80]
EVI2	$(2.92 \times \sqrt{\text{EVI2}} - 0.43)^2$	[73]
	$(3.126 \times \sqrt{\text{EVI2}} - 0.58)^2$	
	$(5.3 \times \sqrt{\text{EVI2}} - 1.66)^{\frac{3}{2}}$	
	$(5.47 \times \text{EVI2}^{\frac{3}{2}} - 1.03)^{\frac{4}{3}}$	
SAVI	$\frac{11 \times \text{SAVI}^3}{-\ln\left(\frac{0.09 - \text{SAVI}}{0.35}\right)}$	[81]
NDVI/IDVI	$(1 - \alpha) \times LAI_{\text{NDVI}} + \alpha \times LAI_{\text{IDVI}}$ $\alpha = \frac{1}{1 + e^{-k \times (\text{NDVI} - 0.8)}}, k \in [12, 20]$	[38]

LAI_{NDVI} and LAI_{IDVI} are estimation results from individual statistical models for each index, applied to the appropriate LAI levels as defined by the author [38].

coefficients: M_{RED} , representing the maximized value of the red waveband, and $f(\Delta)$, the topography adjusting coefficient. The $f(\Delta)$ coefficient, with a value of 2.28, minimizes the mean difference between shadowed and brightly lit inclines. Interestingly, TAVI relies solely on the red and NIR bands, without support from additional topographical data.

Several other index qualities warrant consideration, such as utility for specific value estimations or use as alternatives for other indices [70]. For instance, when estimating fractional vegetation cover, a DVI-based [26] model achieved the highest accuracy and stability [71]. Furthermore, NDVI can be a viable alternative to RVI, which uses radio band data that tends to be costly and difficult to acquire [70]. Finally, NDWI exhibits strong accuracy in estimating vegetation water content, and since a plant's water content is often correlated to its condition, NDWI can serve as a reliable indicator of vegetation health as well [72].

The Leaf Area Index (LAI) is a dimensionless measure that represents the amount of leaf surface area relative to a given ground area. It is not a multispectral index in itself, but is commonly used in plant science, forestry, ecology, and agronomy to quantify vegetation density and is typically expressed as the ratio of leaf area to ground area:

$$\text{LAI} = \frac{\text{Total leaf area}}{\text{Ground area}}$$

LAI has been extensively studied due to its use in ecological and hydrological models [73], [74], [75]. Not considering direct and labor-intensive measuring approaches, beyond the scope of this work, LAI can be estimated through various indirect, multispectral index-based methods, summarized in Table IV. Methods based on combinations of indices have shown superior accuracy and robustness in LAI estimation compared to single index models [38], [76]. Nevertheless, single models for LAI estimation still exhibit significant correlations with observed values, especially in the NIR, red, and blue spectral ranges [69]. Regarding solo models, the literature indicates that models based on NDVI outperform those relying on simple ratio indices, including SR [22] and MSR [29], [77].

B. Soil

Numerous soil characteristics can exert a substantial influence on fire behavior and severity. However, the most relevant are the soil's organic contents [82], [83] and moisture levels [84], [85]. Higher levels of organic matter increase fuel load, making the soil more susceptible to combustion and intensifying the effects of fires. Areas with elevated organic matter content may experience deep-seated and long-lasting underground fires. On this front, a series of studies demonstrated a prediction model supported by several index combinations, including the SR, DVI, NDVI, and GNDVI indexes, reporting high accuracy levels for agricultural soil mapping, with a maximum R^2 of 0.93 [86], [87].

Dry soils contribute to faster fire spread and increased fire intensity. Conversely, moist soils can act as natural dampers, slowing the progression of fires. Simple models using the NDVI and surface temperature for soil moisture estimation have been proposed [88]. However, more recent studies show improved soil moisture estimation accuracy [89], [90] by leveraging indices such as GNDVI [30], SAVI, MSAVI [42], and OSAVI [47]. Other multispectral approaches, which incorporate infrared and thermal data along with more sophisticated analysis algorithms, have also reported good results for soil water content prediction in agricultural settings, including R^2 s upwards of 0.7 [91] and RMSEs as low as 2.5% [92].

C. Water

The presence of water features has two significant impacts on wildfire management: they provide natural firebreaks and serve as essential water sources for firefighting operations. Rapid identification and access to substantial volumes of water, such as lakes, rivers, and reservoirs, are essential for effective fire suppression.

Similarly to the vegetation indexes, water indexes such as the NDWI and MNDWI [42] have their own advantages and disadvantages according to the scenario in question [93]. A study that investigated the performance of solo implementations of the NDWI and MNDWI reported an overall accuracy of 77% and 84.3%, respectively [94] in delineating land surface water features. Moreover, the same study also suggests that fusing vegetation indices with the aforementioned water indices can lead to a reduction in their overall accuracy.

Several machine learning approaches have been developed in an effort to achieve better accuracy and performance in water feature segmentation, including the WatNet [95] and MC-WBDN [96] models, as well as the MuWi¹[97] index. The WatNet model achieved over 95% accuracy in water delineation, surpassing the MNDWI in three selected test regions, which included an urban landscape, a mountainous area, and a vegetated region during high cloud cover. Similarly, the MC-WBDN solution outpaced traditional indices, including NDWI, NDMI, and MNDWI. It achieved the highest performance among all tested methods, with a MIoU of 74.42%, indicating a high probability that a surface water pixel is correctly classified. Finally, MuWi proved its capability to generate

accurate high resolution water maps. The index was validated on six testing sites, showing a higher disposition in classifying non-water as water than the contrary. It displayed overall accuracy exceeding 95% and high statistical significance from the McNemar test, used to determine whether there is a significant difference in proportions on a binary outcome across paired or matched samples [98].

D. Artificial Structures

Artificial surfaces include human-made structures such as buildings, roads, bridges, and other infrastructure, which differ from natural vegetation and terrain in both composition and response to fire. This section focuses primarily on road extraction.

The REI index has achieved accuracy levels of 86% to 88% in extracting asphalt road networks [49]. While this index generally provides useful results, its performance decreases when roads are obscured by trees or shadows, and it has been observed to misclassify building boundaries as roads [49].

Ahmed et al. [50] have also demonstrated high-precision extraction of roads using the RI index. Their proposal successfully detected roads with widths of less than 10 meters in certain regions and has also been able to identify gaps in road features in the presence of buildings and structures made of concrete. In turn, Zhao & Zhu [42] observed how the ASI index improved over seven contemporary indices²—UI [99], NDBI [100], IBI [101], BCI [102], VgNIR-BI [103], PISI [104] and BLFEI [105]—in road extraction over eight study areas, displaying a JMD, TD, and SDI between 2% to 75%, 13% to 164%, and 3% to 131%, respectively.

Finally, the integration of vision algorithms with single indices can enhance the extraction process and minimize misclassifications of roads. For example, the inclusion of machine learning and a data fusion methodology based on majority voting was shown to outperform single indices such as NDVI, NDWI, and SAVI for road extraction on 8 rural, semi-urban and urban environments, with an overall accuracy of 97.78% [106].

E. Burnt Areas

The identification of burnt areas facilitates wildfire damage assessment—in particular the estimation of repercussions on ecosystems and infrastructures—fostering well-informed strategies for post-fire recovery, rehabilitation, and future risk mitigation. Moreover, analysis of the extent and patterns of burnt areas can provide a deeper understanding of the general behavior and characteristics of wildfires within a specific region.

The introduction of the BAI index, which exhibits higher sensitivity to burnt terrain compared to NDVI and SAVI, considerably improved the estimation of burnt areas [107]. However, the same study advises caution when using the index for burned land mapping due to the significant variability within scorched areas. In particular, concerning the use of

¹Formula available in Appendix B, Table XII.

²These and other less common indices are summarized in Appendix B, Table XII and are not discussed in detail in this work.

thresholding techniques, the study recommends the use of one standard deviation of BAI as a threshold, ensuring the most accurate results possible. Furthermore, there is potential for incorporating a shape refinement algorithm after the initial burnt area segmentation process to further improve results.

A subsequent study [108] proposed an NBR-based [37] approach using satellite imagery to detect changes in the extent and severity of burns. Even though it uses the SWIR band—which is typically costly to acquire—the method was particularly successful in comparing results and aggregating information across wide geographical areas and over time.

Finally, Holden et al. [109] highlighted the potential of the NBRT1 [41] index—which directly incorporates thermal reflectance data—in identifying burned areas with low fire-induced vegetation mortality. However, the authors emphasize the need for further research on how the timing of post-fire image acquisition affects the distinction between burned and unburned areas using two- or three-dimensional indices [109].

V. PRACTICAL CASE STUDIES

This section presents two case studies that explore the practical application of multispectral indices for terrain feature extraction. The first case study, detailed in Subsection V-A, conducts an empirical analysis of the results obtained from directly applying selected indices to satellite imagery. The second case study, described in Subsection V-B, extends the analysis by implementing a systematic methodology for index evaluation, facilitating the acquisition of concrete, comparable results for further interpretation.

A. Study I

Study I performs a qualitative assessment of the performance of several spectral indices, including NDVI, NDWI, ARI, MARI, ASI, REI, NBR, and BAI. These indices are derived from satellite reflectance data collected across three distinct regions in Portugal. The analysis focuses on qualitatively evaluating the extent to which each index effectively highlights specific features or phenomena of interest.

1) *Data Collection*: Satellite imagery collection and processing were performed using the Google Earth Engine (GEE) platform [110], facilitating the calculation of selected multispectral indices for designated regions of interest based on Landsat 8 surface reflectance data. For each site under study, a central coordinate point was selected to define the area of interest, from which a bounding square with a side length of 40 kilometers was extracted, yielding a total area of 1,600 square kilometers.

2) *Regions of Interest*: Three regions of interest, illustrated in Fig. 3, were selected for this study due to their diversity and abundance of relevant extractable terrain features, including vegetated areas, water bodies, and urbanized zones. Geographic details for these regions are presented in Table V, and the regions themselves can be described as follows:

A Located within the Lisbon Metropolitan Area, this region features a complex urban and suburban landscape interspersed with significant green spaces and extensive infrastructure. Key geographical features include the

TABLE V
PROPERTIES OF THE REGIONS OF INTEREST FOR STUDY I.

Property	Regions		
	A	B	C
Latitude*	38.7180	37.4453	39.9494
Longitude*	-9.1886	-8.0131	-8.2455
Area (Km ²)	1600	1600	1600

*Coordinates are in the WGS84 standard.

Tagus Estuary on the eastern side, surrounded by urban developments, and its drainage into the Atlantic Ocean to the west. The Sintra mountain range is situated in the northwestern part of the region. Additionally, the area is traversed by two major bridges spanning the Tagus River, underscoring its infrastructural significance.

- B This region in southern Portugal represents a transitional landscape where the sparsely vegetated southern Alentejo region converges with the mountainous ranges of southern Portugal. The northern portion of the area is characterized by a relatively barren, patchwork terrain, reflective of agricultural activities interspersed with natural sparse vegetation. Progressing southward, the terrain transitions into a more rugged and mountainous landscape, with darker hues indicative of denser vegetation and forested areas. This contrast underscores the gradual shift from predominantly agricultural lands to more densely vegetated mountainous regions.
- C Located in central Portugal, this region is characterized by a relatively homogeneous distribution of vegetation. The landscape predominantly consists of a mix of dense forested patches interspersed with open areas, including agricultural lands. A river traverses the region, contributing to its geographical diversity.

3) *Results and Analysis*: The multispectral index maps generated for the regions of interest in Study I are presented in Fig. 4. These maps illustrate the index values using a gradient scale, ranging from low to high, represented by a color scheme transitioning from black to white.

NDVI serves as an indicator of vegetation greenness, with higher values typically denoting dense, green vegetation, and lower values indicating sparsely vegetated or barren areas. This pattern is evident in the analyzed regions. In Region A, urban areas display low NDVI values, reflecting limited vegetation, while green spaces such as the Sintra Mountains and Monsanto Park exhibit high NDVI values, indicative of substantial vegetation cover. Region B demonstrates a pronounced contrast in NDVI values, with the sparsely vegetated northern plains showing low values, and the densely vegetated southern mountainous areas showing high values. This distribution aligns with the spatial arrangement of agricultural activities and natural vegetation. In Region C, relatively homogeneous NDVI values are observed, consistent with a landscape characterized by a mix of forested patches and agricultural lands.

NDWI is most effectively employed to delineate water bodies and evaluate moisture content in vegetation. High NDWI values indicate the presence of water, whereas low values

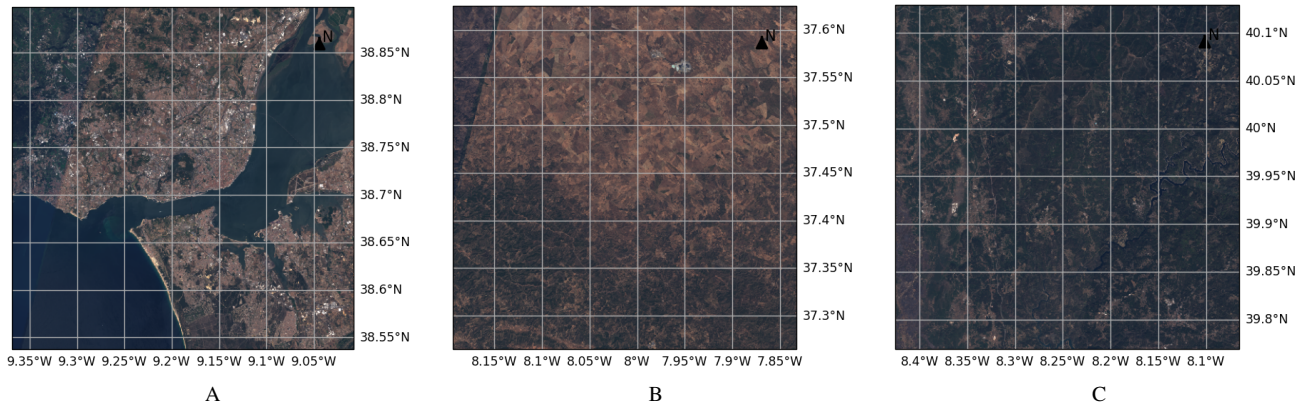


Fig. 3. RGB representation of the three regions of interest in Study I: A – greater Lisbon area; B – southern Portugal; and, C – central Portugal.

correspond to dry conditions or urbanized areas. In Region A, the high NDWI values distinctly outline the Tagus Estuary, in contrast to the low values observed in the surrounding areas, including shallow coastal zones where the riverbed's bottom soil is visible. For Region B, the NDWI map does not reveal significant water presence in the northern areas, consistent with the prevailing arid conditions. However, it highlights the southern region, characterized by dense green vegetation. In Region C, the NDWI map captures some green forested patches but does not prominently distinguish any major water features, excluding the river, albeit very roughly. This limitation may be attributed to insufficient reflectance differentiation between the forested areas and the water.

The ARI and MARI are used to detect the presence of anthocyanins, which impart blue, red, or purple hues to vegetation. Higher values of these indices typically indicate a significant presence of anthocyanins. However, in Regions A, B, and C, a recurring challenge arises: non-vegetative features exhibiting similar spectral characteristics to those associated with anthocyanins are more prevalent than vegetation itself. In Region A, the urban landscape predominates; in Region B, red-toned arid soils to the north are dominant; and in Region C, sparsely vegetated patches exhibit tones resembling those of anthocyanins. While the arid and sparsely vegetated areas in Regions B and C may indeed harbor vegetation rich in anthocyanins, the differentiation power of the indices at this scale proves insufficient for accurate detection.

The ASI and REI indices are designed to focus on artificial structures, with ASI providing a general indication for urban areas and REI targeting roads and similar infrastructure. Higher values of these indices signify the presence of artificial structures, while lower values suggest natural or vegetated areas. In Region A, the ASI index exhibits some similarity to ARI and MARI, but with enhanced differentiation within urban areas, particularly along the major thoroughfares near the coast on both sides of the estuary. Additionally, both bridges are more distinctly recognizable. The REI index, while still emphasizing the two bridges, shows limited differentiation in the remaining urban zones. In Region B, both indices display a similar north-south intensity gradient; however, the differentiation between regions is more pronounced with the

ASI. Notably, no significant urban areas are distinguished in this region. In Region C, ASI highlights the major vegetated or infrastructure. REI presents relatively uniform values across most of the region, except for the bottom-right quadrant, where it clearly delineates the area along the river. ASI shows strong differentiation capabilities for urban areas, particularly large thoroughfares, but its sensitivity to vegetation in proximity to urban zones limits its ability to effectively distinguish these areas. Conversely, REI seems to be overshadowed by the presence of water bodies, such as the Tagus Estuary in Region A and the river in Region C, which diminishes its effectiveness in delineating roads. In Region B, where no significant water bodies are present, REI results align more closely with those of other similar indices.

The NBR and BAI indices are employed to assess fire severity by delineating burned areas. Generally, low values correspond to minimal recent burn activity, whereas higher values indicate the presence of recent fires. Although no recent fire activity is observed in Regions A, B, and C, these indices can still provide valuable insights based on the features they highlight. Burnt areas typically appear dark in multispectral imagery, and these indices are designed to capture such tonalities effectively. The NBR index successfully outlines the darkest features of the imagery across all three regions. In Region A, it emphasizes the water bodies and dense vegetation; in Region B, it accentuates the vegetated southern region; and in Region C, it highlights the dense patches of vegetation and the river. Conversely, the BAI index produces a more homogeneous output. In Region A, it highlights bottom soil near the river shallows; in Region B, it emphasizes the vegetation across the southern region; and in Region C, it functions similarly to NBR, although it seems to capture the darkest areas of the map with greater precision.

B. Study II

Study II expands upon the findings of the first study by quantitatively evaluating the effectiveness of various multi-spectral indices in extracting vegetation, water bodies, and artificial structures from satellite imagery. For each region of interest, a terrain feature map was generated to serve as

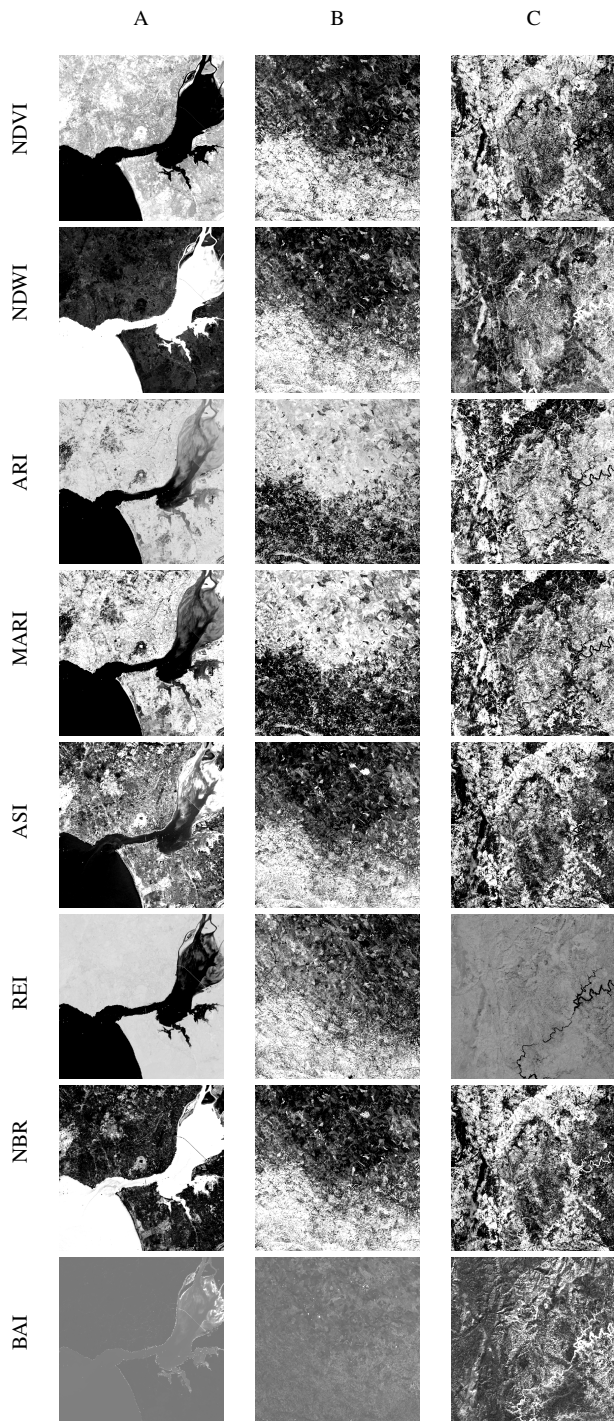


Fig. 4. Study I results. Columns A, B, and C represent three distinct test regions: the greater Lisbon area, southern Portugal, and central Portugal, respectively. Rows correspond to the outcomes of the following indices: NDVI, NDWI, ARI, MARI, ASI, REI, NBR, and BAI.

the ground truth, providing a reliable benchmark for comparison with the processed data. This methodology facilitates the extraction of concrete and statistically significant results, enabling a more objective and robust analysis.

The analysis of multispectral index maps entails calculating the distribution of values within predefined thresholds for a specific extractable feature, using terrain feature maps as masks. The optimal threshold range is identified based on the value distribution of feature-coincident pixels, employing a Gaussian filter for smoothing. This optimal threshold is then applied to the original index map. Finally, the extracted information is compared pixel-by-pixel with the ground-truth terrain feature map, from which segmentation accuracy is computed according to its statistical definition.

1) *Data Collection*: Two resources were obtained from the Portuguese Territory Authority³: the official district geographic shapefiles and the 2022 edition of the official Portuguese land use map [111]. These resources enabled the extraction of land use maps for each district. Additionally, satellite reflectance data from the Sentinel-2⁴ platform were retrieved through the OpenEO API [112], providing the necessary data for computing the multispectral indices for each district.

2) *Regions of Interest*: Portugal is composed of 18 districts (and 2 autonomous regions); from these, four districts, depicted in Fig. 5, were selected based on similar criteria and their approximate geographic proximity to the regions of interest in Study I. These districts, detailed in Table VI and depicted (RGB) in Fig. 5, can be described as follows:

- **Beja** (Fig. 5a): Partially depicted in the northern half of Region B, the Beja district is characterized by vast semi-arid plains, with notable expanses dedicated to viticulture and agriculture.
- **Leiria** (Fig. 5b): Encompassing a portion of Region C, the Leiria district presents a diverse landscape, featuring a coastline, extensive forested areas, and expansive agricultural plains.
- **Lisbon and Setúbal** (Figs. 5c and 5d): These two districts, partially depicted in Region A, are characterized by a blend of urban and suburban areas. Furthermore, they are distinguished by significant coastal regions, natural reserves, and extensive forested areas.

3) *Results and Analysis*: The accuracy results for the distribution of vegetation, water, and artificial structures are presented in Tables VII, VIII, and IX, respectively. The corresponding segmentation threshold values are provided in Table X.

Among the simple greenness indicators (SR to IDVI in Tables VII–X), NDVI, RDVI, GNDVI, GARI, NDRE, and IDVI yielded the best results for vegetation, demonstrating superior accuracy and stability compared to the remaining indices. For water, all greenness indices performed exceptionally well, achieving accuracy values above 97% and standard deviations below 2%, with the exception of MSR, which showed reduced accuracy and markedly higher variability. Conversely, for artificial structures, MSR was the most effective index, delivering

³Direção Geral do Território: <https://www.dgterritorio.gov.pt/>.

⁴ESA Sentinel-2: https://www.esa.int/Applications/Observing_the_Earth/Copernicus/Sentinel-2.

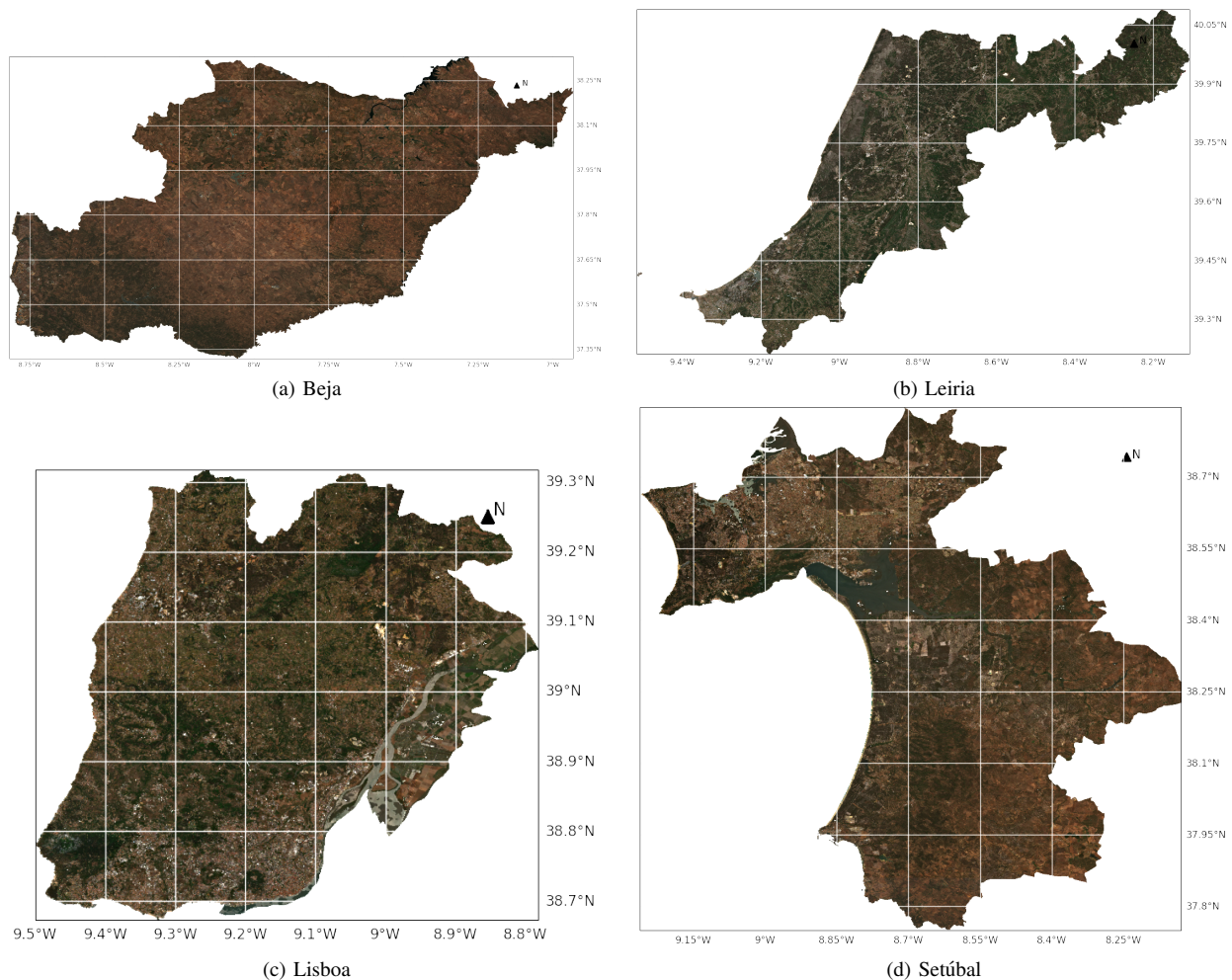


Fig. 5. RGB representation of the four regions of interest: the districts of Beja, Leiria, Lisboa and Setúbal.

TABLE VI
PROPERTIES OF THE REGIONS OF INTEREST FOR STUDY II.

Property	A	B	C	D
Name	Beja	Leiria	Lisboa	Setúbal
Latitude ^a	38.0167	39.75	38.7253	38.5245
Longitude ^a	-7.8667	-8.8	-9.15	-8.8931
Area (Km ²)	10263	3515	2761	5064
Population ^b	147	467	2301	887
Vegetation ^c	51.06%	26.41%	50.89%	36.75%
Water ^c	0.72%	0.13%	2.07%	2.40%
Artificial Structures ^c	0.30%	1.5%	7.74%	1.64%

^aCoordinates are in the WGS84 standard.

^bHundreds of thousands, as of 2022.

^cArea as percentage of entire region.

high accuracy and very low variance, while the remaining indices suffered from either low accuracy, high variability, or, in most cases, both.

The ARI and its modified counterpart, MARI, are designed to accentuate anthocyanin content in vegetation, which is responsible for imparting blue, red, or purple hues. While both indices yielded consistent results overall, ARI outperformed MARI, achieving higher accuracy and exhibiting lower

variability for vegetation ($70\pm3\%$ compared to $40\pm17\%$) and water ($99\pm1\%$ compared to $94\pm4\%$). Particularly for vegetation, it is expected that these indices would show weaker results at this scale, especially during the summer months, when anthocyanin contents are low. For artificial structures, MARI demonstrated better accuracy; however, it was accompanied by significantly higher variability ($65\pm8\%$ compared to $83\pm15\%$).

The EVI and its two-band counterpart, EVI2, both optimized for vegetation analysis, exhibited their best performance for water ($\approx 95\pm2\%$), closely followed by vegetation, which also demonstrated high accuracy and low variability ($84\pm3\%$ and $79\pm8\%$, respectively). However, their performance for artificial structures was notably weaker, with a significant disparity between the two indices ($32\pm22\%$ for EVI and $64\pm23\%$ for EVI2). Among the two, EVI2 achieved superior accuracy, making it the more effective index.

The SAVI and OSAVI indices demonstrated significantly better performance for vegetation ($87\pm4\%$ and $89\pm4\%$, respectively) compared to MSAVI ($54\pm1\%$). However, the reverse was observed for water, where MSAVI achieved the highest accuracy ($99\pm1\%$), slightly outperforming SAVI and OSAVI (both $\approx 97\pm2\%$). For artificial structures, all three

TABLE VII
ACCURACY PERCENTAGE FOR OPTIMAL THRESHOLD RANGES IN
EXTRACTING VEGETATION DISTRIBUTION FOR EACH INDEX AND REGION
OF INTEREST.

Index	Regions				Statistics	
	Beja	Leiria	Lisboa	Setúbal	\bar{X}	σ
SR	56.08	11.00	38.10	46.63	37.95	16.81
NDVI	95.85	89.06	78.36	85.23	87.12	6.33
DVI	54.14	12.80	64.31	61.53	48.20	20.77
RDVI	79.73	65.94	78.18	74.38	74.56	5.34
MSR	45.11	10.55	47.81	47.42	37.72	15.72
GNDVI	94.70	89.16	84.56	90.09	89.63	3.60
GARI	95.52	88.17	82.51	85.01	87.80	4.89
NDRE	95.07	90.91	81.22	88.70	88.98	5.03
GDVI	52.53	45.69	61.96	61.75	55.48	6.82
GRVI	59.17	13.43	45.40	60.39	44.60	18.93
IDVI	93.18	79.50	82.88	89.95	86.38	5.44
ARI	72.23	66.79	66.39	72.39	69.45	2.86
MARI	43.14	10.89	53.08	52.39	39.88	17.19
EVI	87.92	79.76	81.71	85.75	83.78	3.22
EVI2	87.96	82.00	67.44	76.51	78.48	7.55
SAVI	93.17	88.64	84.76	84.19	87.69	3.60
MSAVI	52.79	54.05	53.86	56.76	54.36	1.46
OSAVI	95.44	89.62	85.52	86.20	89.20	3.93
MBI	78.48	57.18	63.33	74.04	68.26	8.44
EMBI	67.59	64.92	69.62	65.28	66.85	1.90
TAVI	55.49	10.79	43.50	46.51	39.07	16.91
NDWI	60.59	10.60	57.72	60.11	47.26	21.19
NDMI	89.57	79.09	63.75	35.52	66.98	20.35
MNDWI	53.55	10.56	54.88	14.34	33.33	20.93
NBR	89.57	79.09	63.75	35.52	66.98	20.35
BAI	95.36	89.63	81.00	85.85	87.96	5.25
AF	95.86	87.92	86.52	91.04	90.34	3.59
VSF	52.87	11.05	47.18	61.30	43.10	19.17
SSF	84.44	77.03	77.20	78.19	79.22	3.05
MF	74.05	61.14	63.67	68.96	66.96	4.97
ASI	95.35	89.69	77.73	85.74	87.13	6.41
REI	70.00	61.88	62.51	69.42	65.95	3.77
RI	95.31	89.58	81.00	85.85	87.94	5.23

TABLE VIII
ACCURACY PERCENTAGE FOR OPTIMAL THRESHOLD RANGES IN
EXTRACTING WATER DISTRIBUTION FOR EACH INDEX AND REGION OF
INTEREST.

Index	Regions				Statistics	
	Beja	Leiria	Lisboa	Setúbal	\bar{X}	σ
SR	99.02	99.36	99.13	98.40	98.98	0.36
NDVI	98.65	99.55	96.71	94.44	97.34	1.96
DVI	98.64	98.97	96.71	94.40	97.18	1.82
RDVI	98.65	99.55	96.70	94.40	97.32	1.98
MSR	96.35	99.17	63.59	67.60	81.68	16.18
GNDVI	98.66	99.55	96.71	94.42	97.34	1.97
GARI	98.66	99.55	96.70	94.44	97.34	1.97
NDRE	98.66	99.54	96.69	94.42	97.33	1.97
GDVI	98.65	99.33	96.71	94.41	97.28	1.91
GRVI	99.31	99.68	99.03	98.19	99.05	0.55
IDVI	98.65	99.55	96.71	94.41	97.33	1.97
ARI	98.81	99.51	98.12	97.55	98.50	0.74
MARI	98.93	97.63	88.11	92.23	94.22	4.33
EVI	98.65	99.55	96.73	94.42	97.34	1.97
EVI2	98.66	99.55	96.71	94.44	97.34	1.96
SAVI	98.66	99.55	96.71	94.43	97.34	1.97
MSAVI	99.34	99.70	98.63	97.58	98.81	0.81
OSAVI	98.66	99.55	96.75	94.48	97.36	1.95
MBI	19.75	99.39	96.70	94.49	77.58	33.43
EMBI	98.63	99.52	96.68	94.35	97.29	1.99
TAVI	98.64	99.16	60.63	94.36	88.20	16.02
NDWI	91.94	99.70	99.18	98.45	97.32	3.14
NDMI	98.65	99.53	27.96	66.36	73.12	29.30
MNDWI	98.50	99.39	98.54	98.12	98.64	0.46
NBR	98.65	99.53	27.96	66.36	73.12	29.30
BAI	1.30	0.40	3.29	5.59	2.64	2.00
AF	98.66	99.55	96.71	94.45	97.34	1.96
VSF	98.65	99.14	94.04	94.49	96.58	2.33
SSF	12.76	99.68	98.80	95.95	76.80	37.00
MF	28.51	81.87	98.26	67.14	68.95	25.81
ASI	1.13	0.69	3.39	6.11	2.83	2.15
REI	68.45	99.54	89.85	94.40	88.06	11.83
RI	1.35	0.45	3.30	5.61	2.68	1.98

indices exhibited comparable accuracy (approximately 50%); however, MSAVI demonstrated much lower variability (4%) compared to SAVI and OSAVI (both $\approx 25\%$).

In terms of accuracy, MBI and its enhanced version, EMBI—which specialize in differentiating soils—exhibited similar performance for vegetation ($\approx 68\%$) and artificial structures ($\approx 45\%$). However, EMBI demonstrated significantly higher accuracy for water (97% compared to 78% for MBI). Additionally, EMBI consistently showed markedly lower variability across all three features, highlighting its improved stability over the MBI.

The TAVI index demonstrated moderate accuracy for water (88 \pm 16%) and artificial structures (76 \pm 10%), but performed significantly worse for vegetation (39 \pm 17%). Notably, despite achieving higher accuracy in some cases, TAVI exhibited substantial variability across all three features, limiting its applicability in real-world scenarios. Designed to mitigate topographical reflectance effects, TAVI may have been disadvantaged in this study as the reflectance maps did not necessitate such corrections, potentially impacting its performance.

The water indices, NDWI and MNDWI, performed expectedly well in water extraction, achieving accuracy values of 97 \pm 3% and 99 \pm 1%, respectively. However, their performance was weaker for vegetation (47 \pm 21% and 33 \pm 21%)

and artificial structures (55 \pm 2% and 63 \pm 7%). In contrast, NDMI, which specializes in detecting vegetation moisture, showed worse accuracy for water (73 \pm 8%) and artificial structures (42 \pm 13%), but achieved better results for vegetation (67 \pm 20%). Despite this, NDMI exhibited high variability across all three features, limiting its reliability.

The NBR and BAI indices were primarily designed for extracting burnt areas. However, since the regions of interest in this study did not feature any recent fire activity, their evaluation for this particular characteristic was not possible. NBR demonstrated mediocre to poor performance across all three features, with accuracy and variability values of 67 \pm 20% for vegetation, 73 \pm 29% for water, and 42 \pm 13% for artificial structures. BAI, while performing poorly for water (3 \pm 2%) and artificial structures (5 \pm 4%), achieved very good results for vegetation (88 \pm 5%). Its performance for vegetation was comparable to dedicated indices such as NDVI (87 \pm 6%), suggesting that BAI could be a viable alternative for vegetation extraction in certain contexts.

The ASI index displayed very good results for vegetation extraction (87 \pm 6%) but performed poorly for artificial structures (13 \pm 17%) and water (3 \pm 2%), ranking among the lowest for these features. Its components—AF, VSF, SSF, and MF—although not designed for direct use as standalone

TABLE IX
ACCURACY PERCENTAGE FOR OPTIMAL THRESHOLD RANGES IN
EXTRACTING ARTIFICIAL STRUCTURE DISTRIBUTION FOR EACH INDEX
AND REGION OF INTEREST.

Index	Regions				Statistics	
	Beja	Leiria	Lisboa	Setúbal	\bar{X}	σ
SR	66.08	88.18	80.58	79.59	78.61	7.96
NDVI	8.16	76.46	70.06	56.00	52.67	26.74
DVI	52.15	74.22	70.64	55.34	63.09	9.50
RDVI	33.80	83.97	73.69	65.48	64.24	18.75
MSR	95.39	94.70	87.72	95.98	93.45	3.34
GNDVI	11.13	55.82	65.78	55.13	46.96	21.11
GARI	13.53	72.95	69.34	50.30	51.53	23.57
NDRE	2.69	71.12	61.18	28.75	40.94	27.07
GDVI	42.44	54.98	57.51	55.81	52.68	5.98
GRVI	67.17	85.71	82.71	84.13	79.93	7.44
IDVI	4.08	49.01	20.78	8.49	20.59	17.51
ARI	51.53	71.85	70.80	66.33	65.13	8.12
MARI	57.85	94.64	87.60	90.60	82.67	14.55
EVI	19.75	70.66	23.50	14.85	32.19	22.42
EVI2	27.88	87.17	77.70	63.23	64.00	22.53
SAVI	15.94	79.39	70.19	56.53	55.51	24.25
MSAVI	44.41	55.27	46.17	47.87	48.43	4.13
OSAVI	9.95	77.02	66.16	41.68	48.70	25.78
MBI	25.68	65.57	47.37	32.69	42.83	15.29
EMBI	45.34	65.33	44.26	40.97	48.98	9.58
TAVI	60.50	88.89	79.99	75.53	76.23	10.28
NDWI	56.01	53.98	52.23	56.50	54.68	1.70
NDMI	37.13	34.84	33.41	64.53	42.48	12.80
MNDWI	55.32	72.79	62.53	59.82	62.62	6.41
NBR	37.13	34.84	33.41	64.53	42.48	12.80
BAI	0.62	5.12	12.32	3.82	5.47	4.28
AF	7.28	43.35	54.80	40.30	36.43	17.68
VSF	58.84	84.41	74.69	71.31	72.31	9.14
SSF	20.87	42.15	34.19	23.09	30.08	8.61
MF	28.53	48.42	39.49	28.97	36.35	8.23
ASI	1.46	5.36	42.36	4.54	13.43	16.77
REI	28.36	44.46	41.89	38.14	38.21	6.12
RI	0.57	5.08	12.32	3.83	5.45	4.29

indices, yielded some notable results. AF achieved excellent accuracy for vegetation and water, but exhibited mediocre performance for artificial structures. Conversely, VSF performed well for water, but showed poor results for vegetation. Both SSF and MF achieved good performance for vegetation but were less reliable for water due to high variability and for artificial structures due to low overall accuracy.

The road extraction indices, REI and RI, demonstrated mediocre to good performance for vegetation extraction ($66\pm 4\%$ and $88\pm 5\%$, respectively). However, their performance varied significantly for other features. For water extraction, RI exhibited much lower accuracy ($3\pm 2\%$) compared to REI ($88\pm 12\%$). Similarly, for artificial structure extraction, RI showed significantly poorer accuracy ($5\pm 4\%$) than REI ($38\pm 6\%$).

VI. DISCUSSION AND RECOMMENDATIONS

It is important to recognize that factors such as regional vegetation composition, environmental conditions, and even the scale of analysis can contribute to the poor performance of certain indices, indicating that they may require further calibration or adjustment for optimal use. Nonetheless, the results obtained in Studies I and II, as well as the literature reviewed

throughout this work, enable us to identify several indices that are particularly effective for specific feature extraction tasks.

The findings from our case studies on vegetation extraction yielded relatively consistent results, with several indices, such as NDVI, GNDVI, GARI, and NDRE, reaffirming their effectiveness by demonstrating high average accuracies and low variability. Interestingly, some indices originally designed for other features, such as BAI, also proved effective for vegetation extraction. In this context, Normalized Difference Vegetation Index (NDVI) stands as our recommended choice. This recommendation is based not only on NDVI's performance in the case studies but also on recent scientific literature supporting its efficacy and widespread use in vegetation cover assessment applications [113], [114], particularly in segmentation tasks [115], [116].

Water extraction was undoubtedly the most competitive category, with the majority of indices—regardless of their specific focus on water extraction—demonstrating exceptional results. This could suggest that the spectral reflectance characteristics of water bodies are more distinct and easier to isolate compared to other land cover types. However, it is important to consider that the relatively small area covered by water in the study region may have influenced these outcomes. In contrast, artificial structures, which also occupy a limited portion of the landscape, did not yield comparable results, suggesting that spatial extent may not be a significant factor contributing to the observed accuracy. Literature identifies MNDWI as a highly effective tool for water extraction [94], a claim that is supported by the findings of Case Study II. MNDWI consistently achieved one of the highest accuracy ratings among the indices evaluated, coupled with low variability, further reinforcing its reliability in this context.

Finally, for artificial structure extraction, all the specialized indices—ASI and its components, REI, and RI—failed to yield satisfactory results. For ASI, the low accuracy and extreme variability observed in Study II raise concerns about the index's overall applicability. In contrast, for the road extraction indices, one could argue that they are primarily suited for road detection rather than artificial structures as a whole. Additionally, at the scale of analysis, the level of road detail may be too fine to capture meaningful results. This argument is further supported by the findings of Study I, where both indices struggled to delineate roads, even major thoroughfares, at a similar scale. While the remaining indices also demonstrate weak and generally unreliable results, MSR emerges as a strong choice for artificial structures, with high average accuracy and low variability, indicating its robust ability to differentiate between artificial structures and other features. However, the optimal threshold range for MSR in artificial structures is incredibly narrow across all features, meaning the decision boundary between the two classes is very tight. While this can result in high precision, as seen in the case, it also suggests that the index may be sensitive to noise, slight variations, or imperfections in the data. Consequently, it might not generalize well to data variations because it has to be finely tuned to such a narrow window.

TABLE X
OPTIMAL THRESHOLD RANGES IN EXTRACTING ARTIFICIAL STRUCTURES, VEGETATION, OR WATER DATA FOR EACH INDEX AND REGION OF INTEREST.

Index	Vegetation				Water				Artificial Structures			
	Beja	Leiria	Lisboa	Setúbal	Beja	Leiria	Lisboa	Setúbal	Beja	Leiria	Lisboa	Setúbal
SR	[-0.01,0.15]	[0.98,1.0]	[-0.16,0.06]	[0.04,0.22]	[-0.26,-0.22]	[-0.18,-0.04]	[-0.23,-0.17]	[-0.16,-0.04]	[-0.03,0.09]	[-0.06,0.06]	[-0.16,-0.04]	[-0.02,0.12]
NDVI	[-0.03,0.01]	[0.02,0.14]	[-0.1,0.06]	[-0.05,0.03]	[0.98,1.0]	[0.98,1.0]	[0.98,1.0]	[0.98,1.0]	[-0.04,0.0]	[-0.04,0.04]	[-0.12,-0.02]	[-0.07,-0.01]
DVI	[0.0,0.22]	[0.9,1.0]	[-0.07,0.21]	[-0.04,0.2]	[0.98,1.0]	[0.98,1.0]	[0.98,1.0]	[0.98,1.0]	[-0.17,0.11]	[-0.05,0.27]	[-0.2,0.0]	[-0.11,0.11]
RDMI	[-0.06,0.06]	[0.16,0.46]	[-0.07,0.15]	[-0.09,0.09]	[0.98,1.0]	[0.98,1.0]	[0.98,1.0]	[0.98,1.0]	[-0.07,0.03]	[-0.08,0.14]	[-0.16,-0.02]	[-0.11,0.01]
MSR	[0.13,0.49]	[0.98,1.0]	[-0.29,-0.05]	[-0.1,0.22]	[-0.34,-0.18]	[0.98,1.0]	[-0.02,0.3]	[-0.05,0.19]	[0.72,1.0]	[0.98,1.0]	[0.98,1.0]	[0.98,1.0]
GNDVI	[-0.03,0.03]	[0.04,0.14]	[-0.05,0.07]	[-0.03,0.05]	[0.98,1.0]	[0.98,1.0]	[0.98,1.0]	[0.98,1.0]	[-0.04,0.02]	[-0.02,0.08]	[-0.1,0.0]	[-0.07,0.01]
GARI	[-0.04,0.02]	[0.01,0.11]	[-0.08,0.06]	[-0.07,0.03]	[0.98,1.0]	[0.98,1.0]	[0.98,1.0]	[0.98,1.0]	[-0.04,0.0]	[-0.05,0.03]	[-0.11,-0.03]	[-0.09,-0.01]
NDR	[-0.03,0.01]	[0.0,0.1]	[-0.08,0.02]	[-0.05,0.01]	[0.98,1.0]	[0.98,1.0]	[0.98,1.0]	[0.98,1.0]	[-0.03,0.01]	[-0.03,0.03]	[-0.09,-0.03]	[-0.07,-0.01]
GDVI	[0.12,0.32]	[0.17,0.49]	[-0.04,0.22]	[0.04,0.26]	[0.98,1.0]	[0.98,1.0]	[0.98,1.0]	[0.98,1.0]	[0.0,0.28]	[0.17,0.49]	[-0.16,0.1]	[-0.15,0.15]
GRVI	[0.07,0.29]	[0.9,1.0]	[-0.08,0.18]	[0.14,0.42]	[-0.41,-0.23]	[-0.21,-0.09]	[-0.31,-0.23]	[-0.21,-0.11]	[-0.04,0.18]	[-0.01,0.19]	[-0.16,0.02]	[-0.02,0.18]
IDVI	[-0.08,-0.04]	[-0.18,-0.1]	[-0.08,-0.04]	[-0.09,-0.05]	[0.98,1.0]	[0.98,1.0]	[0.98,1.0]	[0.98,1.0]	[-0.08,-0.04]	[-0.19,-0.13]	[-0.09,-0.05]	[-0.09,-0.05]
ARI	[0.22,0.42]	[0.41,0.65]	[0.17,0.39]	[0.3,0.54]	[-0.37,-0.33]	[-0.23,-0.19]	[-0.23,-0.03]	[-0.09,0.07]	[0.07,0.31]	[0.2,0.44]	[-0.05,0.19]	[0.13,0.35]
MARI	[0.23,0.55]	[0.95,1.0]	[-0.18,0.12]	[0.1,0.46]	[-0.34,-0.24]	[-0.31,-0.05]	[-0.34,-0.12]	[-0.23,-0.07]	[0.09,0.41]	[0.98,1.0]	[0.82,1.0]	[0.73,1.0]
EVI	[-0.03,0.07]	[0.0,0.1]	[-0.02,0.04]	[-0.02,0.04]	[-1.0,-0.98]	[-1.0,-0.98]	[-1.0,-0.98]	[-1.0,-0.98]	[-0.05,0.03]	[-0.12,0.04]	[-0.04,0.02]	[-0.03,0.03]
EVI2	[-0.04,0.02]	[0.05,0.29]	[-0.1,0.08]	[-0.09,0.05]	[0.98,1.0]	[0.98,1.0]	[0.98,1.0]	[0.98,1.0]	[-0.04,0.0]	[-0.08,0.04]	[-0.14,-0.04]	[-0.09,-0.01]
SAVI	[-0.03,0.01]	[0.03,0.17]	[-0.07,0.07]	[-0.05,0.03]	[0.98,1.0]	[0.98,1.0]	[0.98,1.0]	[0.98,1.0]	[-0.04,0.0]	[-0.05,0.05]	[-0.1,-0.02]	[-0.07,-0.01]
MSAVI	[0.27,0.55]	[0.31,0.61]	[0.13,0.39]	[0.31,0.61]	[-0.36,-0.3]	[-0.24,-0.18]	[-0.48,-0.28]	[-0.34,-0.18]	[0.25,0.55]	[0.45,0.73]	[0.11,0.41]	[0.3,0.6]
OSAVI	[-0.03,0.01]	[0.02,0.14]	[-0.05,0.05]	[-0.05,0.03]	[0.98,1.0]	[0.98,1.0]	[0.98,1.0]	[0.98,1.0]	[-0.04,0.0]	[-0.04,0.04]	[-0.09,-0.01]	[-0.06,0.0]
MBI	[-0.04,0.02]	[0.14,0.34]	[-0.06,0.08]	[-0.05,0.03]	[-0.12,0.02]	[0.98,1.0]	[0.98,1.0]	[0.98,1.0]	[-0.05,0.01]	[0.12,0.36]	[-0.07,0.05]	[-0.04,0.02]
EMBI	[-0.3,-0.06]	[-0.61,-0.31]	[-0.33,-0.11]	[-0.33,-0.11]	[0.98,1.0]	[0.98,1.0]	[0.98,1.0]	[0.98,1.0]	[-0.26,-0.08]	[-0.43,-0.23]	[-0.25,-0.05]	[-0.32,-0.12]
TAVI	[-0.09,0.07]	[0.98,1.0]	[-0.16,0.08]	[-0.08,0.12]	[0.98,1.0]	[0.98,1.0]	[-0.04,0.22]	[0.98,1.0]	[-0.12,0.02]	[-0.11,0.03]	[-0.22,-0.06]	[-0.13,0.03]
NDWI	[-0.01,0.19]	[0.98,1.0]	[-0.04,0.18]	[0.03,0.23]	[0.98,1.0]	[0.98,1.0]	[-0.29,-0.21]	[-0.18,-0.1]	[-0.03,0.13]	[0.14,0.34]	[-0.07,0.13]	[-0.01,0.17]
NDMI	[-0.06,0.11]	[-0.05,0.03]	[-0.14,-0.04]	[-0.12,-0.06]	[0.98,1.0]	[0.98,1.0]	[-0.15,-0.03]	[-0.11,-0.05]	[-0.02,0.06]	[-0.05,0.01]	[-0.14,-0.04]	[-0.12,-0.06]
MNDWI	[-0.06,0.14]	[0.98,1.0]	[-0.02,0.2]	[0.98,1.0]	[0.98,1.0]	[0.98,1.0]	[-0.27,-0.21]	[-0.17,-0.07]	[-0.08,0.11]	[0.08,0.24]	[-0.04,0.12]	[-0.04,0.14]
NBR	[-0.06,0.11]	[-0.05,0.03]	[-0.14,-0.04]	[-0.12,-0.06]	[0.98,1.0]	[0.98,1.0]	[-0.15,-0.03]	[-0.11,-0.05]	[-0.02,0.06]	[-0.05,0.01]	[-0.14,-0.04]	[-0.12,-0.06]
BAI	[-0.33,-0.29]	[-0.54,-0.5]	[-0.28,-0.24]	[-0.41,-0.37]	[-0.33,-0.29]	[-0.54,-0.5]	[-0.28,-0.24]	[-0.41,-0.37]	[-0.33,-0.29]	[-0.54,-0.5]	[-0.28,-0.24]	[-0.41,-0.37]
AF	[-0.03,0.03]	[0.04,0.12]	[-0.03,0.09]	[-0.02,0.06]	[0.98,1.0]	[0.98,1.0]	[0.98,1.0]	[0.98,1.0]	[-0.04,0.02]	[-0.02,0.08]	[-0.1,0.02]	[-0.06,0.02]
VSF	[-0.04,0.22]	[0.97,1.0]	[-0.15,0.09]	[-0.06,0.18]	[-1.0,-0.98]	[0.98,1.0]	[0.39,0.59]	[0.96,1.0]	[-0.18,0.1]	[-0.15,0.09]	[-0.16,-0.02]	[-0.11,0.05]
SSF	[0.27,0.37]	[0.44,0.56]	[0.23,0.33]	[0.34,0.46]	[0.28,0.38]	[-0.17,-0.03]	[-0.34,-0.24]	[-0.21,-0.05]	[0.28,0.36]	[0.45,0.53]	[0.2,0.3]	[0.34,0.46]
MF	[-0.07,0.05]	[0.03,0.19]	[-0.04,0.08]	[-0.05,0.05]	[-0.08,0.04]	[-0.09,0.09]	[-0.11,-0.05]	[-0.06,0.0]	[-0.06,0.04]	[0.04,0.16]	[-0.05,0.07]	[-0.03,0.05]
ASI	[-0.02,0.02]	[-0.01,0.03]	[-0.03,0.03]	[-0.02,0.02]	[-0.03,0.03]	[-0.02,0.02]	[-0.03,0.05]	[-0.02,0.02]	[-0.02,0.02]	[-0.02,0.02]	[-0.03,0.01]	[-0.02,0.02]
REI	[-0.08,0.0]	[-0.06,0.04]	[-0.09,-0.01]	[-0.08,0.02]	[-0.1,-0.04]	[0.98,1.0]	[0.06,0.28]	[0.98,1.0]	[-0.08,0.0]	[-0.08,0.02]	[-0.1,-0.02]	[-0.08,0.0]
RI	[0.29,0.33]	[0.5,0.54]	[0.24,0.28]	[0.37,0.41]	[0.29,0.33]	[0.5,0.54]	[0.24,0.28]	[0.37,0.41]	[0.29,0.33]	[0.5,0.54]	[0.24,0.28]	[0.37,0.41]

VII. CONCLUSIONS

This article presented a review of existing literature on multispectral indices and their applications in extracting specific landscape features, such as vegetation, soil, water, artificial structures, and burnt areas. Additionally, two case studies were presented to assess the effectiveness of key indices selected from the literature, focusing on the extraction of vegetation, water, and artificial structures from satellite imagery.

In the first case study, a qualitative review was conducted to evaluate eight of the most significant indices for various extraction purposes. Their performance was analyzed by examining the output images and considering the foundational principles underlying each index as discussed in the literature. In the second study, a more objective approach was adopted by directly comparing the segmentation outputs of 33 multispectral indices with an official ground-truth land use map. This method enabled the determination of an accuracy rating for each index. Results lead to the identification of the most effective indices for extracting specific landscape features in the regions under analysis. For vegetation extraction, NDVI reaffirmed its position as a reliable choice, demonstrating robust performance consistent with extensive validation in the scientific literature. Regarding water extraction, MNDWI was confirmed as the most consistent and accurate tool for identifying water features. Finally, MSR emerged as the most effective index for extracting artificial structures, demonstrating high accuracy.

Building on these insights, several recommendations for future research can be proposed. A key priority should be gaining a deeper understanding of the regional specificity of each index in relation to particular landscape features. This understanding would enable the more effective use of supporting data, allowing these indices to reach their full potential. Integrating advanced technologies, such as machine learning algorithms and data fusion techniques, holds significant potential to improve the accuracy and reliability of multispectral indices across diverse applications, including those that have shown suboptimal performance [117], [118]. Future studies should explore these approaches to optimize extraction and analysis processes, enabling the generation of more precise and actionable data, especially for critical applications such as wildfire management.

Lastly, while hyperspectral imaging represents a promising frontier in remote sensing for wildfire management, multispectral imaging currently provides the optimal balance of cost-effectiveness and ease of use. Continued research should focus on refining multispectral indices and exploring the integration of hyperspectral data to advance wildfire management strategies, paving the way for more sophisticated and precise monitoring and management solutions.

REFERENCES

- [1] Michaela Korená Hillayová, Ján Holécý, Katarína Korístecková, Marta Bakšová, Milan Ostrihoň, and Jaroslav Škvarenina. Ongoing climatic change increases the risk of wildfires. case study: Carpathian spruce forests. *Journal of Environmental Management*, 337:117620, 2023.
- [2] National Interagency Fire Center. Wildfires and acres statistics, Nov. 22, 2022.
- [3] European Commission. Joint Research Centre. *Forest Fires in Europe, Middle East and North Africa 2020*. Publications Office, LU, 2021.
- [4] Nuno Fachada. A computational pipeline for modeling and predicting wildfire behavior. In *Proceedings of the 7th International Conference on Complexity, Future Information Systems and Risk - COMPLEXIS*, pages 79–84. INSTICC, SciTePress, 04 2022.
- [5] Alexander I Filkov, Thomas J Duff, and Trent D Penman. Improving fire behaviour data obtained from wildfires. *Forests*, 9(2):81, 2018.
- [6] Panagiotis Barmpoutis, Periklis Papaioannou, Kosmas Dimitropoulos, and Nikos Grammalidis. A review on early forest fire detection systems using optical remote sensing. *Sensors*, 20(22):6442, 2020.
- [7] Zhengsen Xu, Jonathan Li, Sibao Cheng, Xue Rui, Yu Zhao, Hongjie He, and Linlin Xu. Wildfire risk prediction: A review. *arXiv preprint arXiv:2405.01607*, 2024.
- [8] David P Roy, Michael A Wulder, Thomas R Loveland, Curtis E Woodcock, Richard G Allen, Martha C Anderson, Dennis Helder, James R Irons, David M Johnson, Robert Kennedy, et al. Landsat-8: Science and product vision for terrestrial global change research. *Remote Sensing of Environment*, 145:154–172, 2014.
- [9] Chein-I Chang. *Hyperspectral data processing: algorithm design and analysis*. John Wiley & Sons, 2013.
- [10] David M Szpakowski and Jennifer LR Jensen. A review of the applications of remote sensing in fire ecology. *Remote sensing*, 11(22):2638, 2019.
- [11] Luis A Pérez-Rodríguez, Carmen Quintano, Elena Marcos, Susana Suarez-Seoane, Leonor Calvo, and Alfonso Fernández-Manso. Evaluation of prescribed fires from unmanned aerial vehicles (uavs) imagery and machine learning algorithms. *Remote Sensing*, 12(8):1295, 2020.
- [12] Wei Li, Dong Li, Timothy A Warner, Shouyang Liu, Frédéric Baret, Peiqi Yang, Jiale Jiang, Mingxia Dong, Tao Cheng, Yan Zhu, et al. Improved generality of wheat green lai models through mitigation of the effect of leaf chlorophyll content variation with red edge vegetation indices. *Remote Sensing of Environment*, 318:114589, 2025.
- [13] Jia Tian, Zhichao Zhang, William D Philpot, Qingjiu Tian, Wenfeng Zhan, Yanbiao Xi, Xiaoqiong Wang, and Cuicui Zhu. Simultaneous estimation of fractional cover of photosynthetic and non-photosynthetic vegetation using visible-near infrared satellite imagery. *Remote Sensing of Environment*, 290:113549, 2023.
- [14] Ali Shamsoddini and Simitkumar Raval. Mapping red edge-based vegetation health indicators using landsat TM data for australian native vegetation cover. *Earth Science Informatics*, 11(4):545–552, April 2018.
- [15] Jia Tian, Shanshan Su, Qingjiu Tian, Wenfeng Zhan, Yanbiao Xi, and Ning Wang. A novel spectral index for estimating fractional cover of non-photosynthetic vegetation using near-infrared bands of sentinel satellite. *International Journal of Applied Earth Observation and Geoinformation*, 101:102361, 2021.
- [16] S. Veraverbeke, I. Gitas, T. Katagis, A. Polychronaki, B. Somers, and R. Goossens. Assessing post-fire vegetation recovery using red–near infrared vegetation indices: Accounting for background and vegetation variability. *ISPRS Journal of Photogrammetry and Remote Sensing*, 68:28–39, 2012.
- [17] Patricia G. Foschi and Huan Liu. Active learning for detecting a spectrally variable subject in color infrared imagery. *Pattern Recognition Letters*, 25(13):1509–1517, 2004. Pattern Recognition for Remote Sensing (PRRS 2002).
- [18] Przemyslaw Polewski, Jacquelyn Shelton, Wei Yao, and Marco Heurich. Instance segmentation of fallen trees in aerial color infrared imagery using active multi-contour evolution with fully convolutional network-based intensity priors. *ISPRS Journal of Photogrammetry and Remote Sensing*, 178:297–313, 2021.
- [19] S. Aronoff. *Remote Sensing for GIS Managers*. ESRI Press, 2005.
- [20] Tiago B. Ramos, Nádia Castanheira, Ana R. Oliveira, Ana Marta Paz, Hanaa Darouich, Lucian Simionesei, Mohammad Farzaman, and Maria C. Gonçalves. Soil salinity assessment using vegetation indices derived from Sentinel-2 multispectral data. Application to Lezíria Grande, Portugal. *Agricultural Water Management*, 241:106387, 2020.
- [21] Dong Zhao and Hao He. Detecting oil slicks under the heterogeneous marine environment utilizing multispectral images. *IEEE Geoscience and Remote Sensing Letters*, 18(5):761–765, 2021.
- [22] Gerald S. Birth and George R. McVey. Measuring the color of growing turf with a reflectance spectrophotometer. *Agronomy Journal*, 60(6):640–643, 1968.
- [23] H. Jiang, Z.-Y. Mao, and X.-Q. Wang. A topography-adjusted vegetation index (tavi) and its application in dynamic forest monitoring. *Beijing Linye Daxue Xuebao/ Journal of Beijing Forestry University*, 33:8–12, 09 2011.

- [24] Jr. Rouse, J. W., R. H. Haas, J. A. Schell, and D. W. Deering. Monitoring Vegetation Systems in the Great Plains with Erts. In *The proceedings of a Symposium held by the Goddard Space Flight Center at Wasgington D.C. on December 10-14, 1973*, volume 351, page 309. NASA Special Publication, 1974.
- [25] Sylvain G Leblanc, Jing M Chen, H Peter White, Josef Cihlar, JL Roujean, and R Lacaze. Mapping vegetation clumping index from directional satellite measurements. In *Proceedings of the Symposium on Physical Signatures and Measurements in Remote Sensing, Aussois, France, 8-13 January*, pages 450-459. CNES Toulouse, France, 2001.
- [26] Compton J. Tucker. Red and photographic infrared linear combinations for monitoring vegetation. *Remote Sensing of Environment*, 8(2):127-150, 1979.
- [27] Zhijun Zhen, Shengbo Chen, Wenhan Qin, Guangjian Yan, Jean-Philippe Gastellu-Etchegorry, Lisai Cao, Mike Murefu, Jian Li, and Bingbing Han. Potentials and limits of vegetation indices with brdf signatures for soil-noise resistance and estimation of leaf area index. *IEEE Transactions on Geoscience and Remote Sensing*, 58(7):5092-5108, 2020.
- [28] Jean-Louis Roujean and François-Marie Breon. Estimating PAR absorbed by vegetation from bidirectional reflectance measurements. *Remote Sensing of Environment*, 51(3):375-384, March 1995.
- [29] Jing M. Chen. Evaluation of vegetation indices and a modified simple ratio for boreal applications. *Canadian Journal of Remote Sensing*, 22(3):229-242, 1996.
- [30] Anatoly A. Gitelson, Yoram J. Kaufman, and Mark N. Merzlyak. Use of a green channel in remote sensing of global vegetation from eosmodis. *Remote Sensing of Environment*, 58(3):289-298, 1996.
- [31] Lifu Zhang, S. Furumi, K. Muramatsu, N. Fujiwara, M. Daigo, and Liangpei Zhang. A new vegetation index based on the universal pattern decomposition method. *International Journal of Remote Sensing*, 28(1):107-124, January 2007.
- [32] Bo cai Gao. Ndwī—a normalized difference water index for remote sensing of vegetation liquid water from space. *Remote Sensing of Environment*, 58(3):257-266, 1996.
- [33] EM Barnes, TR Clarke, SE Richards, PD Colaizzi, J Haberland, M Kostrzewski, P Waller, C Choi, E Riley, T Thompson, et al. Coincident detection of crop water stress, nitrogen status and canopy density using ground based multispectral data. *Proceedings of the fifth international conference on precision agriculture, Bloomington, MN, USA, 1619(6)*, 2000.
- [34] Ravi Sripada. *Determining in-season nitrogen requirements for corn using aerial color-infrared photography*. PhD thesis, North Carolina State University, 01 2005.
- [35] Hanqiu Xu. Modification of normalised difference water index (ndwi) to enhance open water features in remotely sensed imagery. *International Journal of Remote Sensing*, 27(14):3025-3033, 2006.
- [36] Ravi P. Sripada, Ronnie W. Heiniger, Jeffrey G. White, and Alan D. Meijer. Aerial color infrared photography for determining early in-season nitrogen requirements in corn. *Agronomy Journal*, 98(4):968-977, 2006.
- [37] M.J. López García and V. Caselles. Mapping burns and natural reforestation using thematic mapper data. *Geocarto International*, 6(1):31-37, 1991.
- [38] Yuanheng Sun, Huazhong Ren, Tianyuan Zhang, Chengye Zhang, and Qiming Qin. Crop leaf area index retrieval based on inverted difference vegetation index and ndvi. *IEEE Geoscience and Remote Sensing Letters*, 15(11):1662-1666, 2018.
- [39] Emilio Chuvieco and Maria Martín. Cartografía de grandes incendios forestales en la península ibérica a partir de imágenes noaa-avhrr. *Serie Geográfica*, 7, 01 1998.
- [40] Anatoly A. Gitelson, Olga B. Chivkunova, and Mark N. Merzlyak. Nondestructive estimation of anthocyanins and chlorophylls in anthocyanic leaves. *American journal of botany*, 96 10:1861-8, 2009.
- [41] Z. A. Holden, A. M. S. Smith, P. Morgan, M. G. Rollins, and P. E. Gessler. Evaluation of novel thermally enhanced spectral indices for mapping fire perimeters and comparisons with fire atlas data. *International Journal of Remote Sensing*, 26(21):4801-4808, 2005.
- [42] Yongquan Zhao and Zhe Zhu. Asi: An artificial surface index for landsat 8 imagery. *International Journal of Applied Earth Observation and Geoinformation*, 107:102703, 2022.
- [43] Hui Qing Liu and Alfredo R. Huete. A feedback based modification of the ndvi to minimize canopy background and atmospheric noise. *IEEE Transactions on Geoscience and Remote Sensing*, 33:457-465, 1995.
- [44] Zhangyan Jiang, Alfredo R. Huete, Jin Chen, Yunhao Chen, Jing Li, Guangjian Yan, and Xiaoyu Zhang. Analysis of ndvi and scaled difference vegetation index retrievals of vegetation fraction. *Remote Sensing of Environment*, 101(3):366-378, 2006.
- [45] A.R Huete. A soil-adjusted vegetation index (SAVI). *Remote Sensing of Environment*, 25(3):295-309, August 1988.
- [46] J. Qi, A. Chehbouni, A.R. Huete, Y.H. Kerr, and S. Sorooshian. A modified soil adjusted vegetation index. *Remote Sensing of Environment*, 48(2):119-126, 1994.
- [47] Geneviève Rondeaux, M. Steven, and Baret Frederic. Optimization of soil-adjusted vegetation indices. *Remote Sensing of Environment*, 55:95-107, 02 1996.
- [48] Can Trong Nguyen, Amnat Chidthaisong, Phan Kieu Diem, and Lian-Zhi Huo. A modified bare soil index to identify bare land features during agricultural fallow-period in southeast asia using landsat 8. *Land*, 10(3), 2021.
- [49] Kaveh Shahi, Helmi Z.M. Shafri, Ebrahim Taherzadeh, Shattri Mansor, and Ratnasamy Muniandy. A novel spectral index to automatically extract road networks from worldview-2 satellite imagery. *The Egyptian Journal of Remote Sensing and Space Science*, 18(1):27-33, 2015.
- [50] Muhammad Waqas Ahmed, Sumayyah Saadi, and Muhammad Ahmed. Automated road extraction using reinforced road indices for sentinel-2 data. *Array*, 16:100257, 2022.
- [51] Harold Jeffreys. An invariant form for the prior probability in estimation problems. *Proceedings of the Royal Society of London. Series A. Mathematical and Physical Sciences*, 186(1007):453-461, 1946.
- [52] Kameo Matusita. Decision rules, based on the distance, for problems of fit, two samples, and estimation. *The Annals of Mathematical Statistics*, pages 631-640, 1955.
- [53] PH Swain and RC King. Two effective feature selection criteria for multispectral remote sensing. *LARS technical reports*, page 39, 1973.
- [54] Yoram J Kaufman and Lorraine A Remer. Detection of forests using mid-ir reflectance: An application for aerosol studies. *IEEE transactions on geoscience and remote sensing*, 32(3):672-683, 1994.
- [55] Andrew L Sullivan. Wildland surface fire spread modelling, 1990-2007. 1: Physical and quasi-physical models. *International Journal of Wildland Fire*, 18(4):349-368, 2009.
- [56] Andrew L Sullivan. Wildland surface fire spread modelling, 1990-2007. 2: Empirical and quasi-empirical models. *International Journal of Wildland Fire*, 18(4):369-386, 2009.
- [57] Andrew L Sullivan. Wildland surface fire spread modelling, 1990-2007. 3: Simulation and mathematical analogue models. *International Journal of Wildland Fire*, 18(4):387-403, 2009.
- [58] Jeffrey D Colby. Topographic normalization in rugged terrain. *Photogrammetric Engineering and Remote Sensing*, 57(5):531-537, 1991.
- [59] Degui Gu and Alan Gillespie. Topographic normalization of landsat tm images of forest based on subpixel sun-canopy-sensor geometry. *Remote sensing of Environment*, 64(2):166-175, 1998.
- [60] Alexander Berk, Gail P Anderson, Lawrence S Bernstein, Prabhat K Acharya, H Dothe, Michael W Matthew, Steven M Adler-Golden, James H Chetwynd Jr, Steven C Richtsmeier, Brian Pukall, et al. Modtran4 radiative transfer modeling for atmospheric correction. In *Optical spectroscopic techniques and instrumentation for atmospheric and space research III*, volume 3756, pages 348-353. SPIE, 1999.
- [61] Eric F Vermote and Svetlana Kotchenova. Atmospheric correction for the monitoring of land surfaces. *Journal of Geophysical Research: Atmospheres*, 113(D23), 2008.
- [62] Georgia Doxani, Eric Vermote, Jean-Claude Roger, Ferran Gascon, Stefan Adriaensens, David Frantz, Olivier Hagolle, André Hollstein, Grit Kirches, Fuqin Li, et al. Atmospheric correction inter-comparison exercise. *Remote Sensing*, 10(2):352, 2018.
- [63] A. Mummoorthy, R.Roopa Chandrika, N.S.Gowri Ganesh, and E. Pavithra. Satellite image processing biomass estimation. In *2019 International Conference on Emerging Trends in Science and Engineering (ICESE)*, volume 1, pages 1-7, 2019.
- [64] Xiaosong Li, Zhihai Gao, Lina Bai, and Yongxi Huang. Potential of high resolution rapideye data for sparse vegetation fraction mapping in arid regions. In *2012 IEEE International Geoscience and Remote Sensing Symposium*, pages 420-423, 2012.
- [65] Lifu Zhang, Yasuko Mitsushita, Shinobu Furumi, Kanako Muramatsu, Noboru Fujiwara, Motomasa Daigo, and Liangpei Zhang. Universality of modified pattern decomposition method for satellite sensors. In *Asia GIS Conference Publications, Wuhan University, China*, 2003.
- [66] M. Daigo, A. Ono†, R. Urabe, and N. Fujiwara. Pattern decomposition method for hyper-multi-spectral data analysis. *International Journal of Remote Sensing*, 25(6):1153-1166, 2004.

- [67] Xiaojun She, Lifu Zhang, Changping Huang, and Siheng Wang. Comparison of hyperspectral vegetation indices based on casi airborne data. In *2016 IEEE International Geoscience and Remote Sensing Symposium (IGARSS)*, pages 4532–4534, 2016.
- [68] Junxiong Zhou and Jin Chen. Analysis of topographic effects on vegetation indices. In *IGARSS 2019 - 2019 IEEE International Geoscience and Remote Sensing Symposium*, pages 6059–6062, 2019.
- [69] Tian Jingguo, Wang Shudong, Zhang Lifu, Wu Taixia, She Xiaojun, and Jiang Hailing. Evaluating different vegetation index for estimating lai of winter wheat using hyperspectral remote sensing data. In *2015 7th Workshop on Hyperspectral Image and Signal Processing: Evolution in Remote Sensing (WHISPERS)*, pages 1–4, 2015.
- [70] Abdurrahman Gonenc, Mehmet Sirac Ozerdem, and Emrullah Acar. Comparison of ndvi and rvi vegetation indices using satellite images. In *2019 8th International Conference on Agro-Geoinformatics (Agro-Geoinformatics)*, pages 1–4, 2019.
- [71] Kai Yan, Si Gao, Haojing Chi, Jianbo Qi, Wanjuan Song, Yiyi Tong, Xihan Mu, and Guangjian Yan. Evaluation of the vegetation-index-based dimidiate pixel model for fractional vegetation cover estimation. *IEEE Transactions on Geoscience and Remote Sensing*, 60:1–14, 2022.
- [72] Hui Lu, Toshio Koike, Hiroyuki Tsutsui, and Hedeyuki Fujii. Monitoring vegetation water content by using optical vegetation index and microwave vegetation index: Field experiments and applications. In *2011 IEEE International Geoscience and Remote Sensing Symposium*, pages 2468–2471, 2011.
- [73] Yanghui Kang, Mutlu Özdoğan, Samuel C. Zipper, Miguel O. Román, Jeff Walker, Suk Young Hong, Michael Marshall, Vincenzo Magliulo, José Moreno, Luis Alonso, Akira Miyata, Bruce Kimball, and Steven P. Loheide. How universal is the relationship between remotely sensed vegetation indices and crop leaf area index? a global assessment. *Remote Sensing*, 8(7), 2016.
- [74] Roya Mourad, Hadi Jaafar, Martha Anderson, and Feng Gao. Assessment of leaf area index models using harmonized landsat and sentinel-2 surface reflectance data over a semi-arid irrigated landscape. *Remote Sensing*, 12(19), 2020.
- [75] Shenzhou Liu, Wenzhi Zeng, Lifeng Wu, Guoqing Lei, Haorui Chen, Thomas Gaiser, and Amit Kumar Srivastava. Simulating the leaf area index of rice from multispectral images. *Remote Sensing*, 13(18), 2021.
- [76] Kazi A. Kalpoma, Anik Chowdhury, Nowshin Nawar Arony, Mehjabin Nowshin, and Jun-ichi Kudoh. New model vegetation index for boro rice model using 3d plot and k-nn: Bangladesh haor region perspective. In *IGARSS 2019 - 2019 IEEE International Geoscience and Remote Sensing Symposium*, pages 7322–7325, 2019.
- [77] Qiaoyun Xie, Wenjiang Huang, Dong Liang, Pengfei Chen, Chaoyang Wu, Guijun Yang, Jingcheng Zhang, Linsheng Huang, and Dongyan Zhang. Leaf area index estimation using vegetation indices derived from airborne hyperspectral images in winter wheat. *IEEE Journal of Selected Topics in Applied Earth Observations and Remote Sensing*, 7(8):3586–3594, 2014.
- [78] R.B. Myneni, R. Ramakrishna, R. Nemani, and S.W. Running. Estimation of global leaf area index and absorbed par using radiative transfer models. *IEEE Transactions on Geoscience and Remote Sensing*, 35(6):1380–1393, 1997.
- [79] L.F. Johnson, D.E. Roczen, S.K. Youkhana, R.R. Nemani, and D.F. Bosch. Mapping vineyard leaf area with multispectral satellite imagery. *Computers and Electronics in Agriculture*, 38(1):33–44, 2003.
- [80] J.G. Piqueras and Universitat de València. Departament de Física de la Terra i Termodinàmica. *Evapotranspiración de la cubierta vegetal mediante la determinación del coeficiente de cultivo por teledetección: extensión a escala regional : acuífero 08.29 Mancha Oriental*. Tesis doctorals. Universitat de València, Servei de Publicacions, 2008.
- [81] Isabel Pôças, Teresa A. Paço, Mário Cunha, José A. Andrade, José Silvestre, Adélia Sousa, Francisco L. Santos, Luís S. Pereira, and Richard G. Allen. Satellite-based evapotranspiration of a super-intensive olive orchard: Application of metric algorithms. *Biosystems Engineering*, 128:69–81, 2014. Special Issue: Irrigated Agriculture: Water Resources Management for a Sustainable Environment.
- [82] Agustín Merino, Felipe García-Oliva, María T Fontúrbel, and José A Vega. The high content of mineral-free organic matter in soils increases their vulnerability to wildfire in humid-temperate zones. *Geoderma*, 395:115043, 2021.
- [83] Alex Amerh Agbeshie, Simon Abugre, Thomas Atta-Darkwa, and Richard Awuah. A review of the effects of forest fire on soil properties. *Journal of Forestry Research*, 33(5):1419–1441, 2022.
- [84] Erik S Krueger, Tyson E Ochsner, David M Engle, JD Carlson, Dirac Twidwell, and Samuel D Fuhlendorf. Soil moisture affects growing-season wildfire size in the southern great plains. *Soil Science Society of America Journal*, 79(6):1567–1576, 2015.
- [85] David Chaparro, Merce Vall-Llossera, Maria Piles, Adriano Camps, Christoph Rüdiger, and Ramon Riera-Tatché. Predicting the extent of wildfires using remotely sensed soil moisture and temperature trends. *IEEE journal of selected topics in applied earth observations and remote sensing*, 9(6):2818–2829, 2016.
- [86] Long Guo, Peng Fu, Tiezhu Shi, Yiyun Chen, Haitao Zhang, Ran Meng, and Shanqin Wang. Mapping field-scale soil organic carbon with unmanned aircraft system-acquired time series multispectral images. *Soil and Tillage Research*, 196:104477, 2020.
- [87] Long Guo, Xiaoru Sun, Peng Fu, Tiezhu Shi, Lina Dang, Yiyun Chen, M. Linderman, Ganlin Zhang, Yu Zhang, Qinghu Jiang, Haitao Zhang, and Chen Zeng. Mapping soil organic carbon stock by hyperspectral and time-series multispectral remote sensing images in low-relief agricultural areas. *Geoderma*, 398:115118, 2021.
- [88] Inge Sandholt, Kjeld Rasmussen, and Jens Andersen. A simple interpretation of the surface temperature/vegetation index space for assessment of surface moisture status. *Remote Sensing of Environment*, 79(2):213–224, 2002. Recent Advances in Remote Sensing of Biophysical Variables.
- [89] Juntao Deng, Shijia Pan, Mingyu Zhou, Wen Gao, Yuncai Yan, Zijie Niu, and Wenting Han. Optimum sampling window size and vegetation index selection for low-altitude multispectral estimation of root soil moisture content for xuxiang kiwifruit. *Agricultural Water Management*, 282:108297, 2023.
- [90] Smita Rani Swain, Poulamee Chakraborty, Niranjan Panigrahi, Hitesh Bhogilal Vasava, Nukala Nagarjuna Reddy, Sourav Roy, Israr Majeed, and Bhabani Sankar Das. Estimation of soil texture using Sentinel-2 multispectral imaging data: An ensemble modeling approach. *Soil and Tillage Research*, 213:105134, 2021.
- [91] László Bertalan, Imre Holb, Angelika Pataki, Gábor Négyesi, Gergely Szabó, Annamária Kupásné Szalóki, and Szilárd Szabó. UAV-based multispectral and thermal cameras to predict soil water content – a machine learning approach. *Computers and Electronics in Agriculture*, 200:107262, 2022.
- [92] Min-Guk Seo, Hyo-Sang Shin, and Antonios Tsourdos. Soil moisture retrieval model design with multispectral and infrared images from unmanned aerial vehicles using convolutional neural network. *Agronomy*, 11(2), 2021.
- [93] Zhang Fang-fang, Zhang Bing, Li Jun-sheng, Shen Qian, Wu Yuanfeng, and Song Yang. Comparative analysis of automatic water identification method based on multispectral remote sensing. *Procedia Environmental Sciences*, 11:1482–1487, 2011. 2011 2nd International Conference on Challenges in Environmental Science and Computer Engineering (CESCE 2011).
- [94] Mhosisi Masocha, Timothy Dube, Mellisa Makore, Munyaradzi D. Shekede, and Jacob Funani. Surface water bodies mapping in zimbabwe using landsat 8 oli multispectral imagery: A comparison of multiple water indices. *Physics and Chemistry of the Earth, Parts A/B/C*, 106:63–67, 2018.
- [95] Xin Luo, Xiaohua Tong, and Zhongwen Hu. An applicable and automatic method for earth surface water mapping based on multispectral images. *International Journal of Applied Earth Observation and Geoinformation*, 103:102472, 2021.
- [96] Kunhao Yuan, Xu Zhuang, Gerald Schaefer, Jianxin Feng, Lin Guan, and Hui Fang. Deep-learning-based multispectral satellite image segmentation for water body detection. *IEEE Journal of Selected Topics in Applied Earth Observations and Remote Sensing*, 14:7422–7434, 2021.
- [97] Zifeng Wang, Junguo Liu, Jinbao Li, and David D. Zhang. Multi-spectral water index (muwi): A native 10-m multi-spectral water index for accurate water mapping on sentinel-2. *Remote Sensing*, 10(10), 2018.
- [98] Quinn McNemar. Note on the sampling error of the difference between correlated proportions or percentages. *Psychometrika*, 12(2):153–157, 1947.
- [99] Makoto Kawamura. Relation between social and environmental conditions in colombo, sri lanka and the urban index estimated by satellite remote sensing data. *International archives of photogrammetry and remote sensing*, 7:321–326, 1996.
- [100] Yong Zha, Jay Gao, and Shaoliang Ni. Use of normalized difference built-up index in automatically mapping urban areas from tm imagery. *International journal of remote sensing*, 24(3):583–594, 2003.
- [101] Hanqiu Xu. A new index for delineating built-up land features in satellite imagery. *International journal of remote sensing*, 29(14):4269–4276, 2008.

- [102] Chengbin Deng and Changshan Wu. Bci: A biophysical composition index for remote sensing of urban environments. *Remote Sensing of Environment*, 127:247–259, 2012.
- [103] Ronald C Estoque and Yuji Murayama. Classification and change detection of built-up lands from landsat-7 etm+ and landsat-8 oli/tirs imageries: A comparative assessment of various spectral indices. *Ecological indicators*, 56:205–217, 2015.
- [104] Yugang Tian, Hui Chen, Qingju Song, and Kun Zheng. A novel index for impervious surface area mapping: Development and validation. *Remote Sensing*, 10(10):1521, 2018.
- [105] Rafik Bouhennache, Toufik Bouden, Abdmalik Taleb-Ahmed, and Abbas Cheddad. A new spectral index for the extraction of built-up land features from landsat 8 satellite imagery. *Geocarto International*, 34(14):1531–1551, 2019.
- [106] Supattra Puttinaovarat and Paramate Horkaew. Multi-spectral and topographic fusion for automated road extraction. *Open Geosciences*, 10(1):461–473, 2018.
- [107] E. Chuvieco, M. P. Martín, and A. Palacios. Assessment of different spectral indices in the red-near-infrared spectral domain for burned land discrimination. *International Journal of Remote Sensing*, 23(23):5103–5110, 2002.
- [108] Carl Key and Nate Benson. *Landscape Assessment: Ground measure of severity, the Composite Burn Index; and Remote sensing of severity, the Normalized Burn Ratio.*, pages LA 1–51. USDA Forest Service, Rocky Mountain Research Station, 01 2006.
- [109] Z. A. Holden, A. M. S. Smith, P. Morgan, M. G. Rollins, and P. E. Gessler. Evaluation of novel thermally enhanced spectral indices for mapping fire perimeters and comparisons with fire atlas data. *International Journal of Remote Sensing*, 26(21):4801–4808, 2005.
- [110] Noel Gorelick, Matt Hancher, Mike Dixon, Simon Ilyushchenko, David Thau, and Rebecca Moore. Google earth engine: Planetary-scale geospatial analysis for everyone. *Remote Sensing of Environment*, 2017.
- [111] Direção Geral do Território. Serviço nacional de informação geográfica. Accessed on 22/11/2023.
- [112] Florian Lahn. *openeo: Client Interface for 'openEO' Servers*, 2025. R package version 1.4.0, <https://github.com/Open-EO/openeo-r-client>.
- [113] Mohamed Adou Sidi Almouctar, Yiping Wu, Amit Kumar, Fubo Zhao, Koroma John Mambu, and Mohammed Sadek. Spatiotemporal analysis of vegetation cover changes around surface water based on ndvi: a case study in korama basin, southern zinder, niger. *Applied Water Science*, 11:1–14, 2021.
- [114] Yi Cheng, Lijuan Zhang, Zhiqiang Zhang, Xueyin Li, Haiying Wang, and Xu Xi. Spatiotemporal variation and influence factors of vegetation cover in the yellow river basin (1982–2021) based on gimms ndvi and mod13a1. *Water*, 14(20):3274, 2022.
- [115] Petra Bosilj, Tom Duckett, and Grzegorz Cielniak. Connected attribute morphology for unified vegetation segmentation and classification in precision agriculture. *Computers in industry*, 98:226–240, 2018.
- [116] Zhu Ruan, Yaoqiu Kuang, Yeyu He, Wei Zhen, and Song Ding. Detecting vegetation change in the pearl river delta region based on time series segmentation and residual trend analysis (tss-restrend) and modis ndvi. *Remote Sensing*, 12(24):4049, 2020.
- [117] Raúl Hoffrén, María Teresa Lamelas, and Juan de la Riva. Uav-derived photogrammetric point clouds and multispectral indices for fuel estimation in mediterranean forests. *Remote Sensing Applications: Society and Environment*, 31:100997, 2023.
- [118] Chima J Iheaturu, Samuel Hepner, Jonathan L Batchelor, Georges A Agonvonon, Felicia O Akinyemi, Vladimir R Wingate, and Chinwe Ifejika Speranza. Integrating uav lidar and multispectral data to assess forest status and map disturbance severity in a west african forest patch. *Ecological Informatics*, 84:102876, 2024.

APPENDIX A
INDEX ACRONYM TABLE

TABLE XI
MULTISPECTRAL INDICES ACRONYM REFERENCE TABLE.

Acronym	Name
ARVI	Atmospherically Resistant Vegetation Index
ARI	Anthocyanin Reflectance Index
ASI	Artificial Surface Index
BAI	Burning Area Index
BCI	Biophysical Composition Index
BLFEI	Built-Up Land Features Extraction Index
EMBI	Enhanced Modified Bare Soil Index
DVI	Difference Vegetation Index
EVI	Enhanced Vegetation Index
EVI2	Enhanced Vegetation Index 2
FVI	Fusion Vegetation Index
GNDVI	Green Normalized Difference Vegetation Index
HEVI2	Hotspot-Signature 2-Band Enhanced Vegetation Index
HSVI	Hotspot-Signature Soil-adjusted Vegetation Index
IBI	Index-Based Built-Up Index
MARI	Modified Anthocyanin Reflectance Index
MBI	Modified Bare Soil Index
MCARI	Modified Chlorophyll Absorption in Reflectance Index
MNDWI	Modified Normalized Difference Water Index
MSR	Modified Simple Ratio Index
MuWi	Multi-Spectral Water Index
MSAVI	Modified Soil-Adjusted Vegetation Index
MTVI2	Modified Triangular Vegetation Index
NBR	Normalized Burn Ratio Index
NBRT1	Normalized Burn Ratio Thermal Index
NDBI	Normalized Difference Built-Up Index
NDHD	Normalized Difference Between Hotspot and Darkspot
NDMI	Normalized Difference Moisture Index
NDRE	Normalized Difference Red Edge Index
NDVI	Normalized Difference Vegetation Index
NDWI	Normalized Difference Water Index
OSAVI	Optimized Soil-Adjusted Vegetation Index
PISI	Perpendicular Impervious Surface Index
PRI	Photochemical Reflectance Index
RDVI	Renormalized Difference Vegetation Index
REI	Road Extraction Index
REVI	Red-Edge Vegetation Index
RI	Road Index
RVI	Radio Vegetation Index
SAVI	Soil-Adjusted Vegetation Index
SR	Simple Ratio Index
TCARI	Transformed Chlorophyll Absorption in Reflectance Index
TAVI	Topography-Adjusted Vegetation Index
UI	Urban Index
UPDM	Universal Pattern Decomposition Method
VIUPD	Vegetation Index Based on Universal Pattern Decomposition Method
VrNIR-BI	Visible Red and NIR-Based Built-Up Index

APPENDIX B
SUPPLEMENTARY INDEX TABLE

TABLE XII
SUPPLEMENTARY MULTISPECTRAL INDEX TABLE.

Index	Formula	Ref.
UI	$\frac{\rho_{\text{SWIR}2} - \rho_{\text{NIR}}}{\rho_{\text{SWIR}2} + \rho_{\text{NIR}}}$	[99]
NDBI	$\frac{\rho_{\text{SWIR}1} - \rho_{\text{NIR}}}{\rho_{\text{SWIR}1} + \rho_{\text{NIR}}}$	[100]
IBI	$\frac{\rho_{\text{NDBI}} - (\rho_{\text{SAVI}} + \rho_{\text{MNDWI}})/2}{\rho_{\text{NDBI}} + (\rho_{\text{SAVI}} + \rho_{\text{MNDWI}})/2}$	[100]
BCI	$\frac{(H+L)/2 - V}{(H+L)/2 + V}$	[102]
VgNIR-BI	$\frac{\rho_G - \rho_{\text{NIR}}}{\rho_G + \rho_{\text{NIR}}}$	[103]
PISI	$0.8192 \times \rho_B - 0.5735 \times \rho_{\text{NIR}} + 0.0750$	[104]
BLFEI	$\frac{(\rho_G + \rho_R + \rho_{\text{SWIR}2})/3 - \rho_{\text{SWIR}1}}{(\rho_G + \rho_R + \rho_{\text{SWIR}2})/3 + \rho_{\text{SWIR}1}}$	[105]
MuWi	$\sum a_i \rho_i - b$	[105]

$\rho_B, \rho_G, \rho_R, \rho_{\text{NIR}}, \rho_{\text{SWIR}1}, \rho_{\text{SWIR}2}$: Reflectance for the Blue, Green, Red, NIR, and SWIR band reflectances, respectively.

H, V, L: Normalized brightness, greenness, and wetness components from the Tasseled Cap (TC) transformation.

APPENDIX C
 SUPPLEMENTARY PRACTICAL CASE STUDY I FIGURES

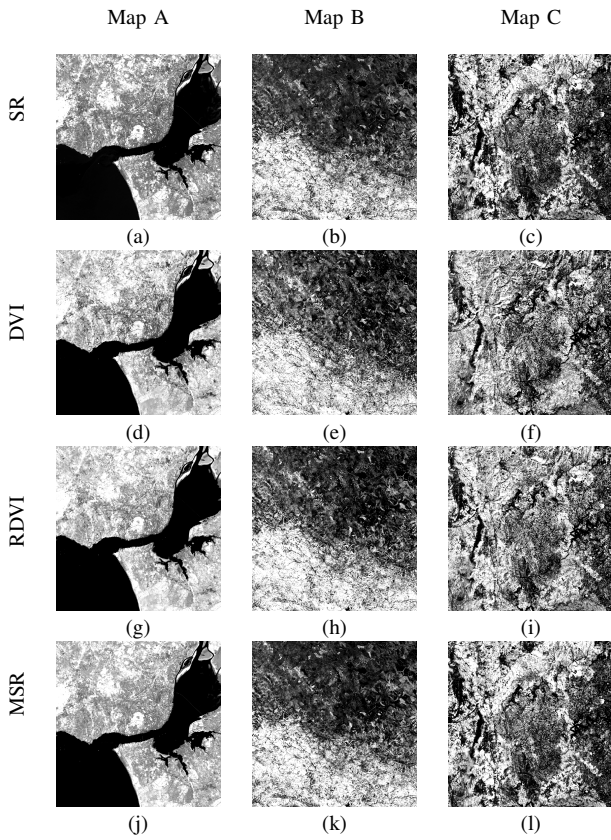


Fig. 6. Case Study I results for the simple greenness indicators (I). Columns A, B, and C represent three distinct test regions: the greater Lisbon area, southern Portugal, and central Portugal, respectively. Every row showcases the outcomes of distinct indices: SR, DVI, RDVI, and MSR.

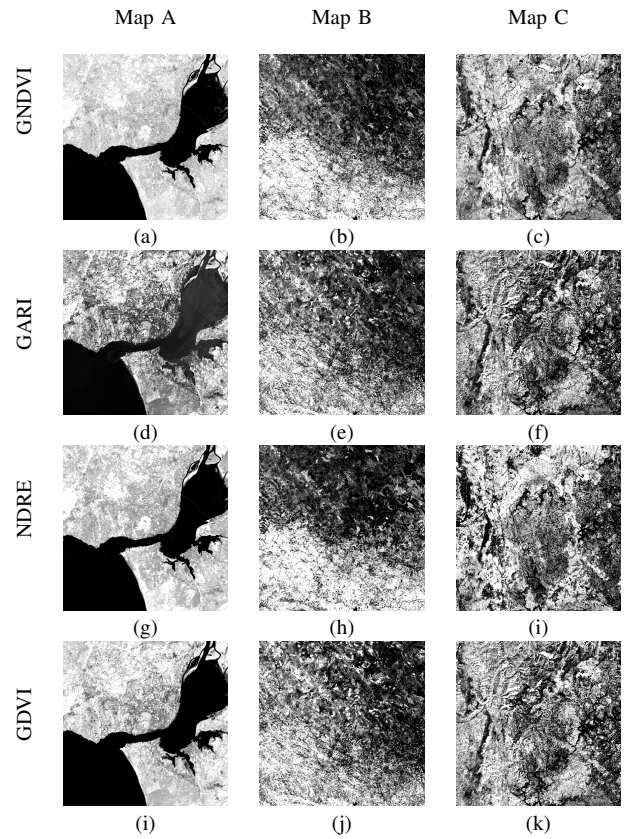


Fig. 7. Case Study I results for the simple greenness indicators (II). Columns A, B, and C represent three distinct test regions: the greater Lisbon area, southern Portugal, and central Portugal, respectively. Every row showcases the outcomes of distinct indices: GNDVI, GARI, NDRE, and GDVI.

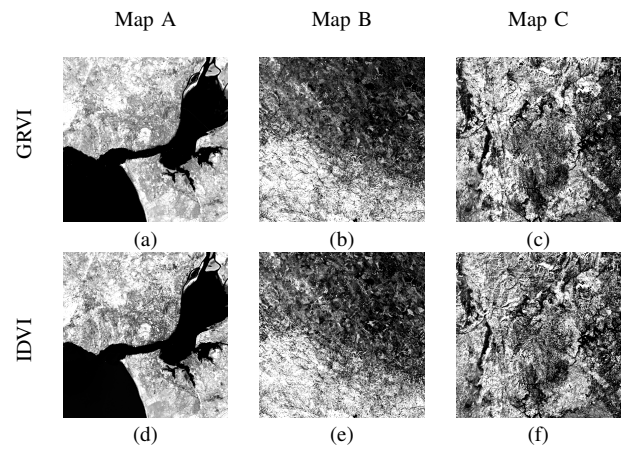


Fig. 8. Case Study I results for the simple greenness indicators (III). Columns A, B, and C represent three distinct test regions: the greater Lisbon area, southern Portugal, and central Portugal, respectively. Every row showcases the outcomes of distinct indices: GRVI and IDVI.

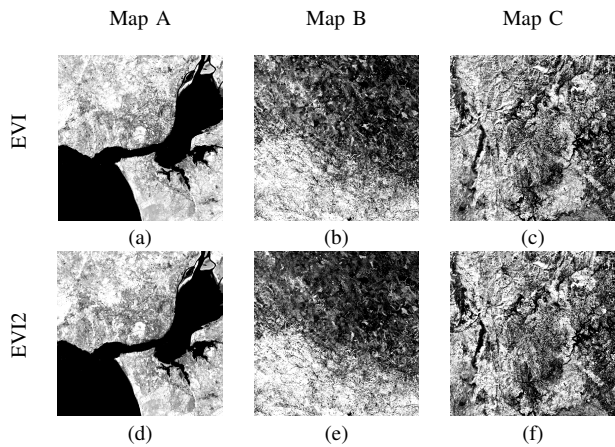


Fig. 9. Case Study I results for the enhanced vegetation indices. Columns A, B, and C represent three distinct test regions: the greater Lisbon area, southern Portugal, and central Portugal, respectively. Every row showcases the outcomes of distinct indices: EVI and EVI2.

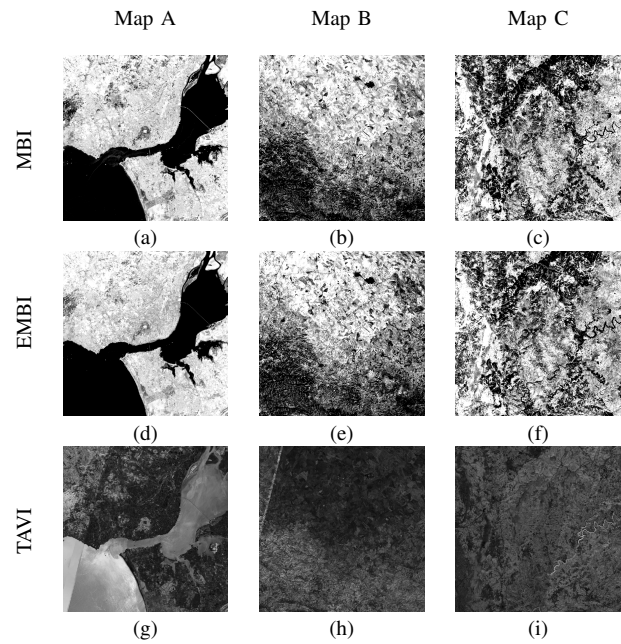


Fig. 11. Case Study I results for the modified bare soil indices and the TAVI. Columns A, B, and C represent three distinct test regions: the greater Lisbon area, southern Portugal, and central Portugal, respectively. Every row showcases the outcomes of distinct indices: MBI, EMBI, and TAVI.

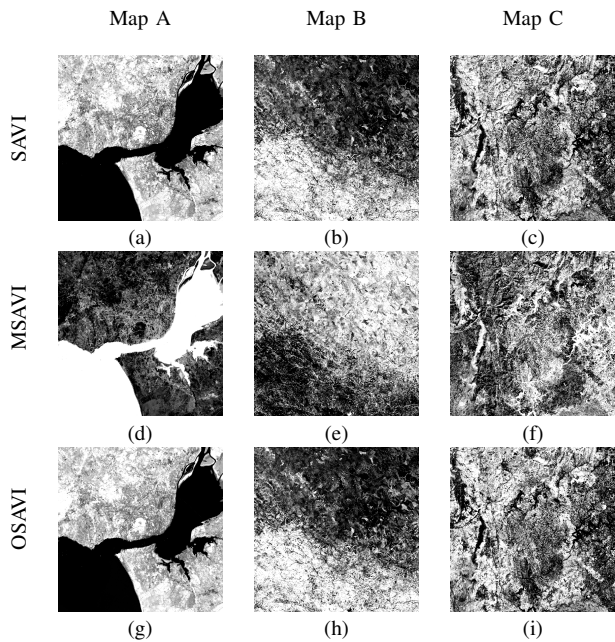


Fig. 10. Case Study I results for the soil-adjusted vegetation indices. Columns A, B, and C represent three distinct test regions: the greater Lisbon area, southern Portugal, and central Portugal, respectively. Every row showcases the outcomes of distinct indices: SAVI, MSAVI, and OSAVI.

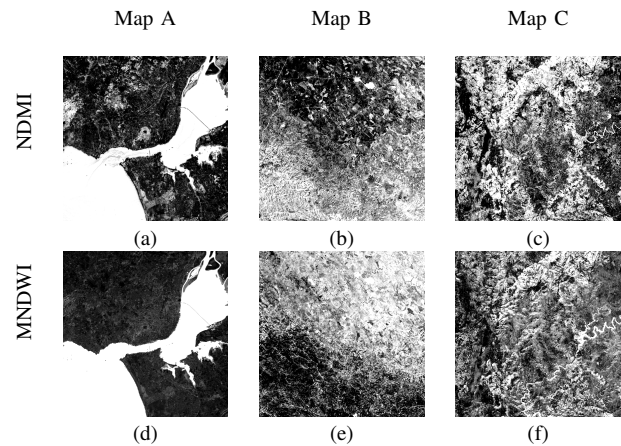


Fig. 12. Case Study I results for the water/moisture extraction indices. Columns A, B, and C represent three distinct test regions: the greater Lisbon area, southern Portugal, and central Portugal, respectively. Every row showcases the outcomes of distinct indices: NDMI and MNDWI.

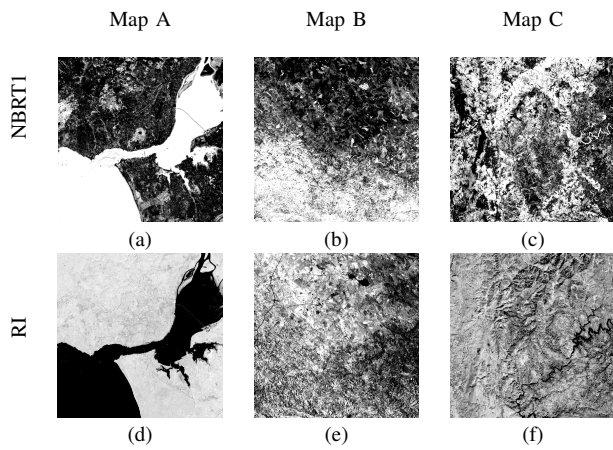


Fig. 13. Practical study results for the NBRTI and RI. Columns A, B, and C represent three distinct test regions: the greater Lisbon area, southern Portugal, and central Portugal, respectively. Every row showcases the outcomes of distinct indices: NBRTI and RI.